Grip Force and Slip Analysis in Robotic Grasp: New Stochastic Paradigm Through Sensor Data Fusion

Debanik Roy
Bhabha Atomic Research Centre
India

1. Introduction

Algorithmic *data fusion* is instrumental in evaluating the quantitative output of a multi-sensory system and the same becomes extremely challenging, especially when the elemental sensory units do vary in type, size and characteristics. Truly, fusion of such *heterogeneous* sensory data remains an open-research paradigm till date, especially in the field of robotics, owing to its inherent characteristics in quantifying the output response of the system. The problem gets even critical when we need to contour with a limited number of elemental sensor-cells (*taxels*), in contrast to traditional theories dealing with large agglomeration of (identical) sensor units. In fact, fusion models used hitherto have been found to be largely inappropriate for the distinct object-groups, e.g. from point-mass to small-sized ones. Besides, paradigms of grasp synthesis (grip force & slippage) were largely unattended. Although traditional theories on sensory data fusion fit quite satisfactorily in searching a pre-defined object with a tentative dimension and depth perception, they fail to do justice in cases where profile of the object do vary from micro-scale to a finite spatial dimension. In answering these lacunas, the present article dwells on modeling, algorithm and experimental analysis of three novel fusion rule-bases, which are implemented in small-sized tactile array sensor to be used in robot gripper. A new proposition has been developed for assessing the *decision threshold*, signaling the *presence of object* inside the grasp-zone of the gripper. Besides, the developed model evaluates the approximate planar area of the grasped object alongwith its shape in real-time. The model also provides estimate for the gripping force required to sustain a stable grasp of the object vis-à-vis slippage characteristics, if any.

Signal detection with multiple sensors, either all similar or dissimilar or any arbitrary combination, can be performed in two manners. In the traditional method, the local sensors communicate all *observations* (raw data) directly to a *centralized detector* (e.g. system controller board) where decision processing is performed. This method, although incorporates parallel channels for data communication, often requires a large bandwidth for the communication channels in order to obtain real-time results. In contrary, the second method deals with each sensor individually, by associating a *detector* module to each of the sensor-cells, which *decides locally* whether a signal is detected or not. These *local decisions* get transmitted to the main controller unit (traditionally called "Data Fusion Center" in the literature), where those get *unified* for *global* decision. Although this method suffers from

loss of information, yet it is the most optimal choice for sensory system design because of high reliability, compact hardware, lower cost and a user-friendly operative environment. In fact, this group of signal processing via localized decision vis-à-vis the field of 'Decentralized / Distributed Decision Making' has been an active area of research, wherein the realization has come out in the manner that these very problems are qualitatively different from the corresponding decision thematic with centralized information. It is, perhaps, wise to conjecture that the prohibitive factor in decentralized problems is not so much the inadequacy of the mathematical tools presently been used, rather the inherent complexity of the problems that have usually been formulated.

The classical theory of optimal sensor signal processing is based on 'Decentralized Testing & Augmentation', using statistical estimation and hypothesis testing methods. The logically driven coherent *unified* output of the said aggregation is being used for processing allied control system signals of the robotic / gripper system. Unlike most of the decentralized control problems, the hypothesis-testing problem can be solved in a relatively straightforward way. This is due principally to the fact that since the decisions made do not get looped back into the system dynamics, those do not affect the information of other decision makers either. However, even in the case of independent observations, several types of unusual behaviour can occur. For example, the threshold computations can yield locally optimal thresholds, which are far from the globally optimal values. The paradigm of decentralized sensor fusion has hitherto been attributed largely by Bayesian Theory, which deals quite robustly the situations involving probabilistic hypothesis testing but fails to address the cases where fuzziness is involved in the main process itself. On the contrary, Dempster-Shafer Theory tackles only those problems where system caters for fuzzy concepts. Unfortunately both of the theories are inadequate so far as the data fusion in mechatronic system is concerned.

We propose a new fusion theory wherein the threshold for fusion can be suitably adapted depending upon the end-application. The proposed schemata provides insight to two aspects, namely evolution of new rule-bases towards data fusion and an optimized inference about object's presence or absence based on stochastic hypothesis testing model. This *dynamic thresholding* of the proposed hypothesis helps fusing the sensory data from the physical device (a multi-input heterogeneous tactile array sensor in the present case), based on the requirement of the user. Moreover, the *fusion rules*, do represent a unique strategy for assimilating the *raw* sensor data. The threshold estimation has been based on using the *variable limits*, exploiting the metrics of Type I error (i.e. rejecting the Alternative Hypothesis when true), as well as Type II error (i.e., accepting the Null Hypothesis when false), corresponding to three different fusion rule-bases. The aim of our work in developing a tailor-made fusion-based hypothesis is concentrated on two vital aspects, viz. it should be able to i] *cater large number of sensor-cells*, which are heterogeneous in nature and ii] *sense the presence of tiny 'point-objects'* on the gripper surface. It may be mentioned that both of these two paradigms were overlooked in the researches hitherto and thus, the existing fusion cum hypothesis testing models are unsuitable to real-life applications in robotics. In the contrary, our model of data fusion and statistical hypothesis testing with new threshold thematic will ensure reliable measure towards overall *qunatization* (e.g. overall external shape, surface area and approximate contour) of the object(s) present in the vicinity of the gripper. In our model, hypotheses are postulated corresponding to different types of sensory outputs. Here, we will differ from the traditional nomenclatures for Null Hypothesis (H_0) as "Signal is

absent" against Alternative Hypothesis (H_1) as "Signal is present", in order to suit our requirement towards robotic grasp-based situations. We, therefore, define the hypotheses as *Significant Object Present* [SOP] vs. *Significant Object Absent* [SOA] respectively for 'H_1' and 'H_0'. We define "Significant Object" as those objects whose surface area is larger than that of the graspable area of the gripper or in other words, larger than the sensing area of the gripper. We prefer to adhere to the bi-modal hypothesis paradigm and represent the inherent *fuzziness* in decision-making process with *white noise*, having a relatively higher value of Signal-to-Noise Ratio (SNR). Three novel *Fusion Rule-bases*, viz. [a] *Multiplicative,* [b] *Additive* and [c] *Preferential Selection,* have been formulated in order to reveal the inter-cell relationship of the array (matrix) sensor. In other words, these rule-bases are devised to represent the exact way the elemental cells (*taxels*) are 'reacting' with one another. We will finally have a logical *unified* output from the system controller using these rule-bases and individual signal-output from the taxels. The *dynamic (global) threshold*, as proposed in our model, is to be selected optimally using the user-specified value of either probability of Type I error or Type II error. The filtered sensory data is used to estimate the optimal value of the grip force, which is required to be applied by the jaw to maintain stable vis-à-vis slip-free farm grasp. Nonetheless, the developed model will also ensure the user regarding the characteristics of the post-grasp slip, if any.

Although traditional surveillance problem with multiple sensors and optimization therein using log-likelihood function have been addressed substantially in last two decades (Chair & Varshney, 1986) & (Gustavo & Grajal, 2006), it lacks generality in situations of sensing 'point-objects'. These algorithms are based on an approach wherein maximum likelihood of remotely located unknown signal(s) can be estimated under white Gaussian noise, but the techniques can't be adopted for sensing *localized* sensor-signals.

Field-sensor outputs in a distributed tracking vis-à-vis surveillance system are categorized in two broad groups, depending on a] the *modus operandi* or activation syntax (parallel or serial) and b] the physical layout (staggered or synchronous). Unlike the case of distributed decision making in parallel, fusion problem with the configurations of sensors in serial chain (Viswanathan et al, 1988), (Hashemi & Rhodes, 1989) & (Swaszek, 1993) may have better performance over the parallel distribution case for two sensors. However, the methods perform poorly for large sensor-cells, which is the typical case in real-life applications. Likewise, a comparative study on the system performance was made using temporally staggered sensors as well as synchronous sensors, using a novel metric, namely, average estimation error variance (Niu et al, 2005). Irrespective of the *modus operandi*, serial or parallel, selection of *local node* in a distributed sensor network is crucial, as it will govern the decision-making system regarding the incorporation of the corresponding data for surveillance (Kaplan, 2006).

Tracking of remote target using multiple field-sensors is a well-researched field, irrespective of its genesis; vide *static target* [e.g. a rigid sensor rig] (Chroust & Vincze, 2004) or *maneuvering target* (Jeong & Tugnait, 2005). In case of static targets, e.g. presence of objects in the vicinity of the gripper-sensor, an estimation of the bias in outputs of the asynchronous field-sensors is important. The decoupling between the numerical estimations for the target state and the sensor bias is attained, considering, a] the cross-covariance between the state & bias estimates (Lin et al, 2005) and b] the reduced bias estimate of the joint probabilistic data association (JPDA) algorithm (Kalandros & Pao, 2005). However, for large number of sensor-cells, like the case of ours, the performance of the distributed tracker has been found

degrading in comparison to centralized estimation, despite using optimal track-to-track fusion algorithm (Chen et al, 2003).

In contrast to log-likelihood method, the fusion tests to be adopted for achieving maximized probability of detection (for a fixed probability of false alarm) should ideally be Neyman – Pearson [N-P] (Srinivasan, 1986). Nonetheless, the threshold of N-P test becomes data dependent if the conditional impedance is removed (i.e. hypotheses are not truly statistically independent) and does not yield any easy solution for optimization (Tsitsiklis & Athans, 1985). Moreover, N-P fusion rule needs the sensor error probabilities (i.e. probability of false alarm & probability of miss) to be known a-priori and those must not be altered during the fusion process. These are very stringent preludes to the decision paradigms that degrade the performance of the data fusion (El-Ayadi, 2002).

The solution of data fusion problem for fixed binary local detectors with statistically independent decisions (Chair & Varshney, 1986) was amplified and extended for i] correlated local binary decisions (Moshe, 1992) and ii] team hypothesis testing and environmental simulation (Tenney & Sandell, 1981a), (Sadjadi, 1986), (Reibman, 1987), (Papastavrou & Athans, 1992) or iii] multidimensional data association (Kirubarajan et al, 2001), (Gan & Harris, 2001); iv] covariance control (Kalandros & Pao, 2002) and v] new design for low-bandwidth track fusion (Ruan & Willett, 2005). In fact, the fused decision in a distributed data fusion problem for similar as well as dissimilar sensors using N–P test is transmitted alongwith a quality information in numerical terms, viz. 'degree of confidence' (Thomopoulos et al, 1987). Various methodologies, such as *extended Kalman filter* (Nabaa & Bishop, 1999), *layered neural networks* (Karniely & Siegelmann, 2000) or *Bayesian estimation* (Okello & Challa, 2004) have been postulated towards fixing sensor alignment problems (known as sensor registration in the literature) in distributed fusion, unlike the method of maximum likelihood estimator, used hitherto.

Another school of thought in fusion optimization is using time-varying global threshold, which essentially calls for the solution of two coupled sets of dynamic programming equations for computation (Tenney & Sandell, 1981b,c), (Teneketzis & Varaiya, 1984) & (Tang, 1991). The case of decentralized detection system with feedback and memory using the Bayesian formulation is investigated (Alhakum & Varshney, 1996), wherein the optimization gets summed up in a likelihood ratio test at the local detectors for statistically independent observations. However, the process gets computationally intensive once the system has a large number of sensors (Moshe et al, 1991). Although the universality of Bayesian approach is recognized for computational transparency (Moshe et al, 1999), yet a few specific situations are better analyzed either through Dempster - Shafer theory (Murphy, 1998) or another novel theory (Thomopoulos, 1990), which gives a good trade-off between the Bayesian and D-S approaches. Interestingly, the inherent uncertainty in a two-hypothesis model is also alleviated in a recent research, by considering a discrete decision zone between Null & Alternate Hypothesis (Wang, 1998). However, irrespective of the major three techniques used in hypothesis testing, e.g. Log-likelihood Ratio [LLR], N-P or D-S, one lacuna is surfacing that the potential of Type I and Type II error shielding is not utilized to a proper extent. But these two cut-offs, i.e. Type I & Type II error can be of significant relevance in defining global thresholds and to be specific, this potential has been used in our architecture. Our methodology essentially involves a *non-parametric stochastic adaptive decision fusion*, wherein fusion center knows only the number of the sensors under each sub-types, but does not consider their error probabilities. In contrast to non-stochastic

fusion algorithms, e.g. (El-Ayadi, 2002), our technique uses a hypothesis error-based global threshold for the final decision regarding the *target* (i.e. presence of object near the graspable zone of the robot gripper).

The first two rule-bases and the developed hypothesis, described here, have been tested with an indigenous tactile array-sensor, comprising three types of taxels, namely, resistive cells (*R-cells*), capacitive cells (*C-cells*) and piezo cells (*P-cells*) placed in matrix. The sensor has got 61 elemental taxels in total, each of which provides calibrated output (in mV) when excited with external forcing. However, we will consider the readings from 57 taxels, which will be sufficient for experimental investigation. Out of these 57 taxels, 32 taxels belong to R-cells, while C-cells & P-cells constitute 21 & 4 taxels respectively. The sensor has been simulated for two-jaw grasp (i.e. considering it as a gripper-sensor) and experimented with a variety of objects imping over it. The sensory output is processed for the determination of object's presence alongwith its size & shape and used for the evaluation of grip as well as slip force. On the other hand, the *Preferential Selection* rule-base was tested through a two-jaw sensor-instrumented robotic gripper, having 18 heterogenous taxels in total, distributed in three categories, viz. load cells (*L-cells*), thin-beam sensors (*TBS-cells*) & infrared sensors (*IR-cells*), bearing 2, 10 & 6 taxels respectively.

2. Hypothesis testing and proposed schemes of data fusion

2.1 Formulation of statistical hypothesis

We prefer to adhere to the bi-modal hypothesis paradigm and represent the inherent *fuzziness* in decision-making process with *white noise*, having a relatively higher value of Signal- to -Noise Ratio (SNR). Nonetheless, these two hypotheses have been re-modeled from real-life perspective as shown below,

$$H_0 : X_i = N_i \tag{1}$$

$$H_1 : X_i = S + N_i, \quad \forall \, i = 1,2,3,\ldots,n$$

where, X_i : Observation vector of the $i^{th.}$ sensor; N_i : Noise vector at the $i^{th.}$ sensor; S: Actual detectable signal vector; n: Total number of sensors in the system. The a-priori probabilities of 'H$_0$' and 'H$_1$' are: $P(H_0) = P_0$ and $P(H_1) = P_1$. We assume all of these 'i' detectors ($\forall$ i=1,2......,57 in case of matrix sensor & i=1,2..,18 for jaw-gripper) have observations at the individual detector level, denoted by, X_i. Now, each detector employs a "Decision Rule", in order to make a decision-vector 'u_i', which is the *localized* logistic metric. Let, logistic parameter, $\{u_i\}$, $\forall$ i=1,2......57 or 18, be defined against individual sensor-cells, such that, u_i= -1, if H$_0$ is true and = + 1, if H$_1$ is true. We also consider the activation syntax of the data fusion to follow *serial* path. Nonetheless, the set $\{u_i = +1\}$ is to be arrived at by considering a cut-off value, ζ, in the following manner,

$$\{u_i = +1\} = \{\forall u_i \Vdash u_{s+}\} \tag{2}$$

where, u_{S+} is mapped as,

$$u_{s+} \xrightarrow{\quad mapping \quad} (X_i - N_i) \geq \zeta \tag{3}$$

and,

$$[X_i] - [N_i] = [Y_i] \tag{4}$$

We further assume that the observations at the individual detectors are statistically independent and the conditional probability density function is described by, $P(Y_i / H_k)$, $\forall i=1,2,\ldots,57$ or 18 $\&\forall k=0,1$. The stated propositions are equally valid for $\{u_i\} = [0,1]$ tuple $\forall i=1,2,\ldots,n$, wherein "0" signifies truth of H_0 and "+1" is correlated to occurrence of H_1. Nonetheless, the Global U, viz. 'U_G' will be a function of all the elemental fused data, i.e., 'u_i'. In other words, it essentially means that the global fused data, $\{U_G\}$, is an extrinsic function of $\{u_i\}$, i.e. $\{U_G\} = f(u_1, u_2,\ldots, u_N)$, where $N=57$ or 18, depending upon the total number of taxels. The proposed method of inference relies on a 'variable limit' or *dynamic threshold*, which is to be estimated through a mathematical model. The location of the dynamic threshold limit is dependent on the confidence level for rejecting 'H_1', chosen a-priori, i.e. on the numerical value of Type I or Type II error.

2.2 Development of fusion rules
2.2.1 "k-out-of-n" logic revisited
Before detailing out the proposed application-oriented fusion rules, we would examine the "k-out-of-n" logic, used hitherto as a quick reference to the evaluation of fusion hypothesis. The rule verdicts "presence of object" if 'k' or more detectors select 'H_1' at the elemental detection level out of total 'n' detectors. As a matter of fact, considering the set of 'u_i' as $\{u_i\}=[-1,1]$, for first two rule-bases, U_G is syntaxed as,

$$U_G = +1, \text{ if } (u_1 + u_2 + \ldots + u_{57}) \geq 2k - n$$

$$= -1, \text{ otherwise.}$$

Although the rule clearly demarcates the acceptance or rejection of 'H_1' in case of large objects (i.e. objects having planar area sufficiently more than that of the sensing area), it fails to demarcate adequately the occurrence of 'point-force', unless we define $k=1$ a-priori. It may be stated that barring its marginal limitations, this logic has been imbibed by most of the decentralized fusion metric, by and large. However, the bottleneck in fusion problem with "k-out-of-n" logic can be tackled more elegantly using the concept of threshold, as used in Bayesian estimation theory. Our rules will hence follow the *Global Thresholding* principle in evaluating the test hypotheses. However, in contrast to "k-out-of-n" logic, the new rules will propose acceptance or rejection of 'H_1' on the basis of numerical value of U_G and the value of *dynamic threshold* considered in that situation. By definition, it is the global threshold only, but we call it *dynamic* as its value gets changed depending upon the application environment. This dynamic threshold can be evaluated numerically from the system parameters, known a-priori. Thus, in true sense, the new rules are functionally in inverse proposition with respect to "k-out-of-n" logic.

2.2.2 Syntax of the fusion rules developed
The first two novel *Fusion Rule-bases*, viz.*Multiplicative* and *Additive,* have been formulated in order to reveal the inter-cell relationship of the matrix sensor, while the third one, i.e. *Preferential Selection*, is aimed at revealing the inter-cell relationship of the semi-matrix layout of the jaw gripper sensors. In other words, these rule-bases have been devised to represent the exact way the taxels are 'reacting' with one another, i.e. in what way these taxels are 'influencing' the neighbouring taxels and/or getting influenced by those. We will finally have a logical *unified* output from the system controller, considering the set of 'u_i' as

$\{u_i\}$=[-1,1]. All the three rule-bases culminate in a non-zero value of U_G for $\{u_i\}$=[-1,1] and the evaluation is *unbiased* so far as the object-size is concerned.
The Multiplicative model defines 'U_G' as,

$$U_G = \prod_{i=1}^{i=n} e^{u_i} = (e)^{n-2k} \tag{5}$$

while, the Additive model postulates the definition of 'U_G' as,

$$U_G = \sum_{i=1}^{i=n} u_i = (n - 2k) \tag{6}$$

where, $\{u_i\}$: localized decision for the ith taxel, $\forall i$ =1,2,….n; 'n': total number of taxels activated in the sensor and 'k': number of taxels giving output as "-1", i.e. "signal absent".
Now, the *fused* decision regarding the selection of test hypothesis will be ruled by the evaluation paradigm, decided a-priori. In our model, we use the numerical value of the *dynamic threshold* ($\lambda_{Threshold}$) as the evaluation metric. We define the evaluation metric for both of the models as: if $U_G \geq \lambda_{Threshold}$, then accept H_1, otherwise reject H_1. In a similar manner, we can obtain the values of U_G using $\{u_i\}$=[0,1] tuple for multiplicative and additive models also. For multiplicative model, the value of U_G will be e^{n-k} and for additive model the value of U_G will be equal to (n-k).
Now, we define 'U_G' under Preferential Selection model as,

$$U_G = \sum_{i=1}^{i=n} u_i (1 + u_{i+1})^p (1 + u_{i-1})^q \tag{7}$$

where, $\{u_i\}$: localized decision for the ith taxel, $\forall i$ =1,2,….n; 'n': total number of taxels activated in the gripper sensor system; p: relative weightage of the succeeding taxel, i.e. $(i+1)^{th}$ cell and q: relative weightage of the preceding taxel, i.e. $(i-1)^{th}$ cell, where $0 \leq p,q \leq 2$. Exact numerical values of p & q need to be ascertained from experimentation with the sensory modules of the jaw-gripper. In that respect, eqn 7 is in a generalized format, which can be adapted for other similar systems as well. We also assume that in eqn. 7, $\{u_{i-1}\}_{|i=1} = 0$ and $\{u_{i+1}\}_{|i=n} = 0$. It may be noted that this model is essentially taxel-specific, unlike the previous models (vide eqn. 5& 6), wherein cumulative effect of the taxels are reflected only. In contrast, the *relative dependency* of one taxel over the neighbouring ones is getting priority in the present model. Hence, we have christened this model as *'preferential selection'*, as the effect of adjoining taxels can be taken into consideration towards computing U_G, depending upon their relative influence/ importance. It may be stated that, this model, by definition, is best suited for taxels arranged in a row or column-wise fashion, i.e. applied for *row /column matrix*. Also, taxels may or may not be equally likely; nonetheless, we are unsure about the outcome (-1 or +1) of a specific taxel in the *grid*. It may be mentioned additionally here that the effect of relative dependency of the taxels could also be considered by another *sister-model* of U_G, viz. $U_G = \sum u_i (1- u_{i+1})^p(1- u_{i-1})^q$, but it would have been rather difficult to be interpreted graphically. Now, so far as the evaluation is concerned, we use the *dynamic threshold band* and the numerical value of the *mean threshold* ($\lambda_{Threshold-mean}$) as the evaluation metric in this rule-base. We define the evaluation metric as: if $U_G \geq \lambda_{Th-mean}$, then accept H_1, otherwise reject H_1. But, alongwith discrete acceptance / rejection, we will also encounter

one *fuzzy-zone*, which will signify *in-decision* regarding the acceptance or rejection of H_1. Numerically, this in-decision zone will be directly proportional to the width of the threshold-band. It may be noted from eqns. 5 & 6 that the value of 'k' carries significance so far as the relative implications of it on P (H_1) is concerned. Figure 1 shows the schematic view of the variation of $P(H_1)$ with 'k'. The first plot we considered is a simple straight-line plot while the other two are exponential fits.
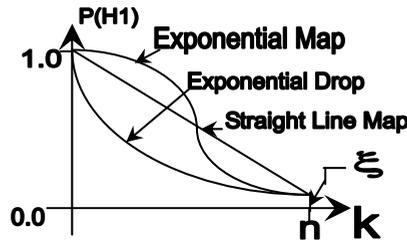
Fig. 1. Probability curves as per the fusion rules proposed

Based on the curves shown above, the mathematical formulae for evaluating $P(H_1)$ or in short, 'p' will be as follows,

$$p = \left(\frac{\xi - 1}{n}\right)(k) + 1 \quad \text{[For straight-line map]} \tag{8}$$

and,

$$p = \exp\left(\frac{\ln \xi}{n}\right)(k) \quad \text{[For exponential curves]} \tag{9}$$

2.2.3 HEBTEM: new strategy for selecting dynamic threshold

The *dynamic threshold*, as proposed in our model, is to be selected optimally using the user-specified value of either probability of Type I error or Type II error. It is termed as "Hypothesis Error Based Threshold Evaluation Method" **(HEBTEM)**. The proposed method relies on the selection of the confidence level, as stipulated by probability of Type I or Type II error. However, we use probability of Type I error as the confidence level for additive model of fusion rule-base and probability of Type II error as the same for multiplicative model. For example, in case of multiplicative model of fusion, estimation using "2% non-confidence level" (i.e. probability of Type II error as 0.02) essentially declares the situation of 'object presence' with 98% certainty. We shall now investigate the situations in order to select the dynamic threshold using HEBTEM.

2.2.3.1 *Using Multiplicative Model*

Here, in-line with eqn. 9, an exponential curve has been fitted for the plot of $P(H_1)$ vs. U_G. The plot uses $\{u_i\}=[-1, +1]$ tuple and the generic representation of the *probability curve* is shown in fig. 2a. Similarly, we can get the plot of $P(H_1)$ vs. U_G for $\{u_i\} = [0,1]$ tuple too (refer fig. 2b). We assume that the probability of alternative hypothesis, i.e. $P(H_1)$ to be 0.5 when nearly half of the sensor-cells (i.e 'n/2') will show "signal present", i.e. the value of 'k' becomes 'n/2' and that of U_G is 1.0. The final decision about "acceptance" and "rejection" of alternative hypothesis will be based on the location of global threshold (λ_{Th}) and the

observed value (represented as x' in fig. 2) of U_G. The scale along the X-axis of the plot also depicts the increment of U_G from e^{-n} to e^n, corresponding to the variation of 'k', from n to 0. We also assume that at k = n, i.e. when all the sensor-cells are giving {u_i}=-1, the occurrence of an object is *minimal*, which is quantified through 'ξ'. The numerical value of 'ξ' is kept very small, in the order of 0.002 to 0.004, as found suitable for the matrix sensor. In fact, 'ξ' is the true indication of the presence of 'point-mass' or 'point-force' over the gripper surface. Thus, we can identify two representative points in the plot, viz. (e^{-n}, ξ) and (e^n, 1.0), which will be decisive in using the plot analytically.
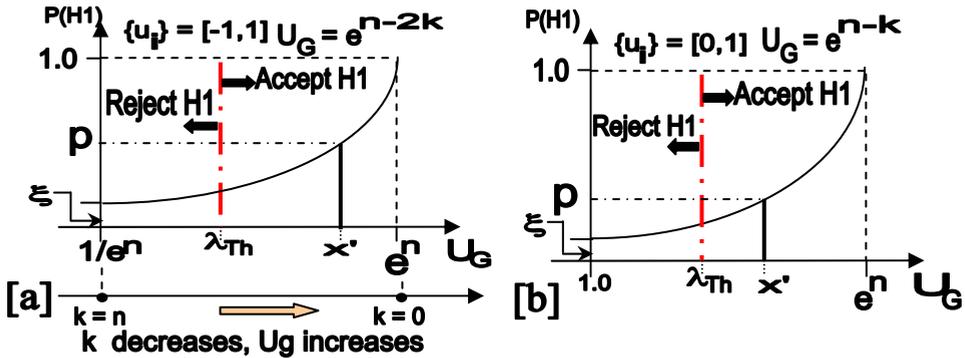
Fig. 2. HEBTEM with multiplicative model of data fusion for [a] {u_i}=[-1,1] & [b] u_i}=[0,1]

As part of two-point interpolation for the exponential curve shown in fig. 2a, we consider the following transcendental equation involving ξ, viz.

$$P(H_1) \equiv p = a\exp^{mU_G} \tag{10}$$

It may be observed from the above equation that the value of both 'm' and 'a' can be evaluated numerically if 'ξ' is known, vide,

$$m = \frac{e^n \ln\left(\dfrac{1}{\xi}\right)}{\left(e^{2n} - 1\right)} \tag{11a}$$

and

$$\ln\left(\frac{1}{a}\right) = \frac{e^{2n} \ln\left(\dfrac{1}{\xi}\right)}{\left(e^{2n} - 1\right)} \tag{11b}$$

2.2.3.2 *Using additive model*

Additive model of fusion rule-base considers probability of Type I error as the basis for ascertaining the presence or absence of object on the gripper. A graphical representation of the probability curve, using HEBTEM, is plotted in fig. 3 considering {u_i}=[0,1] tuple. Considering an exponential fit for the probability distribution shown in fig. 3, the probability of alternative hypothesis becomes,

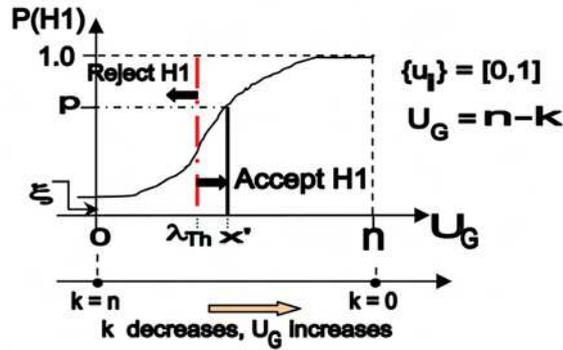$$P(H_1) \equiv p = \xi \exp^{\frac{\ln\left(\frac{1}{\xi}\right)}{n} U_G} \tag{12}$$

Fig. 3. Probability curve for additive model of fusion rule with $\{u_i\}=[0,1]$ using HEBTEM

However, paradigms of P (H_1) plot changes significantly for $\{u_i\}=[-1,+1]$ tuple (refer fig. 4).
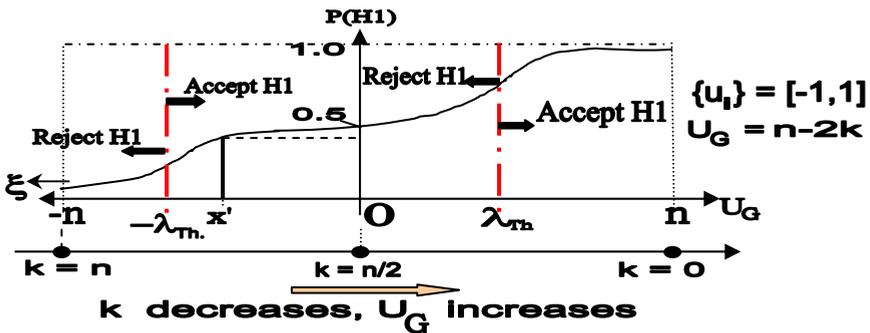

Fig. 4. Probability curve for additive model of fusion rule with $\{u_i\}=[-1,1]$ using HEBTEM

As articulated before, ξ symbolizes the presence of 'point-mass' or 'point-force' over the gripper surface. Here we can identify three representative points in the plot, viz. $(-n, \xi)$; $(0, 0.5)$ and $(n, 1.0)$, which will be used in formulating the transcendental equation involving ξ in order to evaluate P (H_1). We will use a generic equation for the exponential curve, viz. p $=$a. $e^{mx} + cx$, where 'p'=P(H_1); 'x' =U_G and 'm' & 'c' are constant functions of ξ. The final equation, after three-point interpolation as stated above, becomes,

$$P(H_1) \equiv p = 0.5 \exp^{\frac{\ln\left[(\xi+1)+\sqrt{\xi(\xi+2)}\right]}{n} U_G} + \left[\frac{1-0.5\{(\xi+1)+\sqrt{\xi(\xi+2)}\}}{n}\right] U_G \tag{13}$$

It is to be noted from eqn. 13 that we will use only positive values of 'm' and 'c', discarding the theoretically possible negative values of those. Also, unlike fig. 4, here we can use either of the two thresholds, namely '$\lambda_{Th.}$' or '-$\lambda_{Th.}$', depending upon the application environment. In case we use a positive value for '$\lambda_{Th.}$', i.e. right-hand side of the curve, then the decision regarding the rejection /acceptance of 'H$_1$' will be restricted to the right-hand-side zone of

the curve only. Likewise, if we intend to use the negative value for '$\lambda_{Th.}$', our decision has to be within the left-hand-side zone of the curve. Thus, in a way, additive model with $\{u_i\}=[-1,+1]$ tuple advocates *symmetric thresholding*, but not occurring simultaneously.

2.2.3.3 *Using preferential selection model*

A graphical representation of the probability curve for 'H_1' as per this model is plotted in fig. 5 considering $\{u_i\}=[-1,1]$ tuple. Here we will characterize the threshold-band with three parameters, namely: 'A': $\lambda_{Th\text{-}initial}$; 'B': $\lambda_{Th\text{-}final}$ & the mid-point of the band as: $\lambda_{Th\text{-}mean}$.
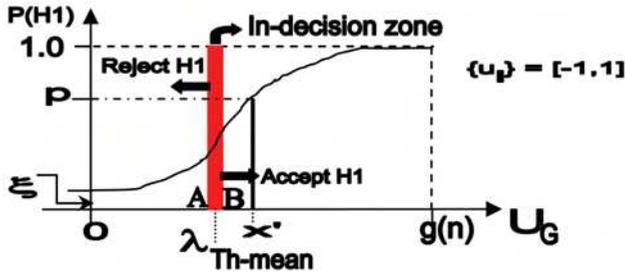

Fig. 5. Probability curve for the preferential selection model using HEBTEM

Using an exponential fit for the probability distribution shown in fig. 6, we have,

$$P(H_1) \equiv p = \left[\frac{1-\xi}{\{g(n)\}^2} \right] U_G{}^2 + \xi \tag{14}$$

In eqn. 14, ξ symbolizes the presence of 'point-mass' or 'point-force' over the gripper surface and $g(n)$ signifies the gamut of the maximum possible values of U_G for various numerical combinations of (p,q). The function $g(n)$ can be computed using the format of U_G, viz.

$$U_G = (2^p + 2^q) + (n-2)[2^{(p+q)}], \quad \forall u_i = +1 \tag{15}$$

As per eqn 15, the values of $g(n)$, in ascending order will be, $\{g(n)\}$: {(2n-1), (4n-5), (4n-4), (8n-10), (16n-24).....} for various combinations of (p,q), where $\{p,q\} \subset [0,2]$. Figure 6 explains the geometric interpretation of $g(n)$, in evaluating U_G. Successive values of $g(n)$ are interpreted   serially as $[g(n)]_1$, $[g(n)]_2$,....$[g(n)]_k$, which becomes the yard-stick for the flattening of the probability curve, keeping ξ unaltered through-out.

2.2.3.4 *Analysis of the Rule-bases and Evaluation of Dynamic Threshold*

Major advantage of the proposed method, viz. HEBTEM, lies with the fact that it doesn't include the concept of *Bayesian Risk*, which inherently involves the computation related to Probability of False Alarm (P_f) and Probability of Miss (P_m). The concept of *Bayesian Risk* is suitable only to cases where a large group of field-sensors are either attempting to evaluate the presence or absence of a single object or *tracking* a single *target*. In such a situation, all of the field-sensors do participate in the decision-making process and the output of each one of those will definitely be biased by its own $[\{P_f\}-\{P_m\}]$ tuple. But, in situations like robotic grasping or stand-alone tactile sensing, the use of sensor-cells will be governed by the actual size, shape and contour of the object to be 'sensed' and/or grasped.
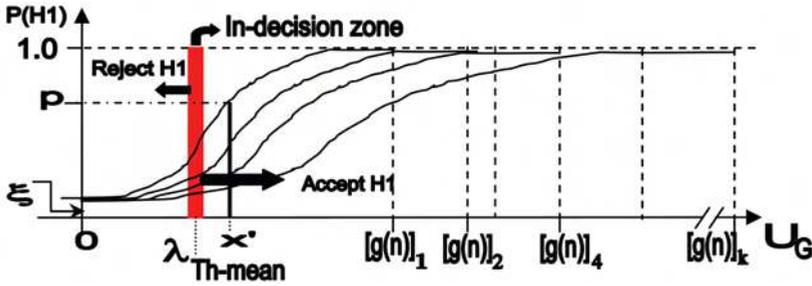
Fig. 6. Variation of probability curves under different tuples of the model

The value of the *dynamic threshold* (viz. λ_{Th} in figs. 2 to 4) can be estimated using either of the models, namely, multiplicative or additive. However, the paradigm of evaluation is different in these two cases. While multiplicative model of the fusion rule-base considers a non-confidence level (β), the additive model considers a confidence level (α), both chosen a-priori. It may be noted that the confidence level (α) for the additive model is nothing but the accepted level of probability of Type I error and 'β' is the probability of Type II error. Figure 7 illustrates the philosophy of HEBTEM, wherein we have shown the zones of certainty and uncertainty for selecting 'H_1'. Here by 'f (x)' we mean the exponential curve for $P(H_1)$, vide eqns. 10, 12 & 13, i.e. corresponding to multiplicative & additive models using [-1,1] tuple.
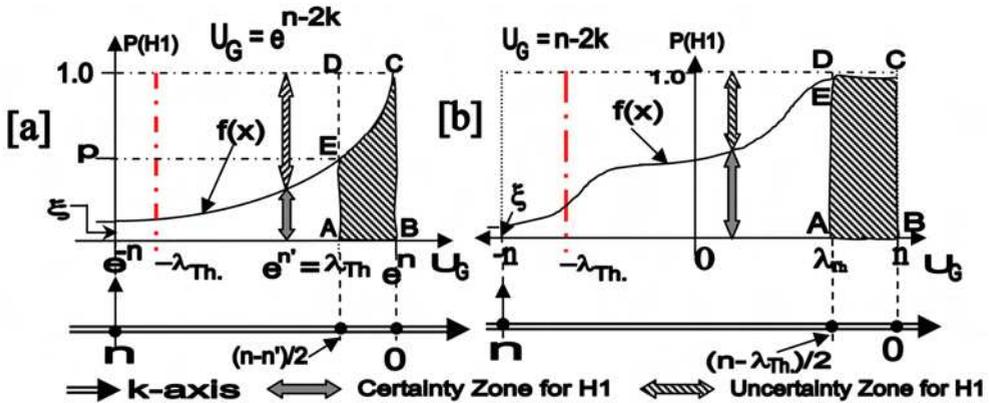

Fig. 7. Computation of dynamic threshold using [a] multiplicative & [b] additive model

It may be stated here that using an exponential fit for the multiplicative model is advantageous, because we can use a wider range of 'λ_{Th}' with almost the same numerical value of 'β'. Thus in order to interpret the presence of *point-force /point-object*, it is wiser to consider such a 'λ_{Th}', which is *closer* to the origin (i.e. the point with k=n). For these cases of point-force selection, the usual value of 'β' will be quite large, because there will be a high tendency of selecting 'H_0' (refer the plots of fig. 2). With reference to fig. 7, the dynamic threshold is evaluated mathematically using multiplicative model as,

$$\int_{\lambda_{Th}}^{e^n} f(x)dx = [1-\beta]\left(e^n - \lambda_{Th.}\right) \tag{16}$$

and the same is computed using additive model as,

$$\int_{\lambda_{Th}}^{n} f(x)dx = [1-\alpha]\left(n - \lambda_{Th.}\right) \tag{17}$$

where, n: Total number of sensor-cells in the system and x: Individual decision vector of the sensor-cells. Both of these two equations are powerful in the sense that on simplification, these culminate in transcendental equations for '$\lambda_{Th.}$', which will finally produce two values for '$\lambda_{Th.}$', one positive and the other negative. So, depending upon the nature of our application, we can select either '+$\lambda_{Th.}$' or '-$\lambda_{Th.}$'. The details of the computations for the above two equations are presented in *Appendix I*.

It may be noted that the formulation of the multiplicative model inherently leads to the inference for 'H_0', especially when the object-size is very small (i.e. 'k' is large). That means, there is always a natural tendency towards selecting 'H_0' *wrongly* and thereby committing a *Type II error*. Hence we need to consider the probability of Type II error, 'β' in computing the required area (under hatch, refer fig. 7), and subsequently, '$\lambda_{Th.}$'. In contrast to this, the additive model suggests equally likely outcome, i.e. the model can select 'H_1', but may commit a *Type I error* by *rejecting* it too. That means, here we must consider the probability of Type I error, 'α' in computing the desired area and the factor, $(1-\alpha)$ in eqn. 17 denotes the level of confidence we have in selecting the 'H_1'.

However, choice of 'α' or 'β' will largely depend upon the value of 'n', i.e. how large the sensor-cell system is or to that extent, how big is the sensor-matrix. Nevertheless, a *stricter* level (i.e. lower value of α or β) will lead to a tougher strategy for accepting the alternate hypothesis, viz. "signal is present". So, depending upon the exact use of the sensor system, 'α' or 'β' can be selected. For example, for a gross gripping of a comparatively large object we need not have a stricter confidence level and hence, even a probability of Type I error of 10% may be allowed in such a case. However, that won't be the right choice when the same sensory system is being used as a *stand-alone system* detecting *point-force*, instead of being augmented with the robot gripper. Hence, the user can take a final decision regarding the actual presence of object by analyzing $P(H_1)$, as obtained from the models.

Unlike the distinct value of the dynamic threshold as per the evaluation pattern proposed in fig. 7, the preferential selection model dictates the *dynamic threshold-band* (viz. $\lambda_{Th\text{-}mean}$ in fig. 5), as described earlier. It can be estimated using the statistical confidence level (α), i.e. probability of Type I error, as stated below. Here 'x' & 'f(x)' represent individual decision-vector of the taxels and the exponential curve for $P(H_1)$, vide eqn. 14 respectively, while $[g(n)]_s$ signifies the maximum value of U_G ($\forall s=1,2,\ldots.k$).

$$\int_{\lambda_{Th-mean}}^{g(n)_s} f(x)dx = [1-\alpha][g(n)_s - \lambda_{Th-mean}] \tag{18}$$

The planar area of the threshold-band, i.e. the *fuzzy-area* of *in-decision* can be computed as,

$$\int_{\lambda_{Th-initial}}^{\lambda_{Th-final}} f(x)dx = \int_{\lambda_{Th-initial}}^{g(n)_s} f(x)dx - \int_{\lambda_{Th-final}}^{g(n)_s} f(x)dx = [1-\alpha][\lambda_{Th-final} - \lambda_{Th-initial}] \tag{19}$$

and the width of the threshold-band ($\delta\lambda_{Th}$) is defined as the numerical difference between $\lambda_{Th\text{-}final}$ and $\lambda_{Th\text{-}initial,}$ i.e. ($\lambda_{Th\text{-}f} - \lambda_{Th\text{-}i}$) and modeled as,

$$\delta\lambda_{Th} = \frac{\alpha}{4} g(n) \qquad (20)$$

However, choice of 'α' will largely depend upon the value of 'g(n)', i.e. how intense is the effect of relative dependency in the sensor-matrix or to that extent, how large is (p,q) tuple. Nevertheless, a *stricter* level (i.e. lower value of α) will lead to a tougher strategy for accepting the alternate hypothesis, viz. "object is present".

2.2.3.5 *Fusion optimization: advantage HEBTEM*

HEBTEM, augmented with our fusion models, has been found advantageous over the traditional optimization techniques followed hitherto, namely, [a] Log-likelihood Ratio Test (LLR) and [b] Neyman-Pearson (N-P) Test. These techniques, though used vastly in situations concerning distributed data fusion problems, do possess inherent drawbacks. Both of these methods simply rely on the basic fact that both 'P_0' and 'P_1' are un-biased, i.e. in case of a new data fusion problem, such as the detection of the object-presence by the gripper sensor, both 'H_0' and 'H_1' are equally likely to occur. However, this pre-assumption of equally likeliness of the hypotheses is not valid for situations like robotic grasping and sensing the presence of object in the gripper-jaw. With regard to grasp analysis, there can be two domains of hypothesis metric, which has got *in-built biasing,* e.g. a] situations where either 'H_0' or 'H_1' is biased and b] situations where 'H_0' or 'H_1' are associated with penalty coefficients. In fact, neither LLR nor N-P test is fit for handling these two environments with impeding bias. We shall now investigate these situations in detail.

a.   *Situations where either 'H_0' or 'H_1' is biased*
For an un-biased equally likely situation, the ratio between P_0 and P_1 is always 1.0, because the probabilities of both null and alternate hypotheses are 0.50. Mathematically it implies,

$$P_0 / P_1 = P(H_0) / P(H_1) = 1.0 \qquad (21a)$$

and

$$\text{we denote,} \quad \lambda_0 = P_0 / P_1 \qquad (21b)$$

This ratio between P_0 and P_1 is being used to compute g*lobal threshold* (λ_0) for the fusion problem, in general. As per equation (21b), the working formula for λ_0 will simply be the ratio between P_0 and P_1 in all *equally likely* cases, wherein the numerical value for the global threshold will be 1.0. However, since the numerical value of λ_0 is the deciding factor for both LLR and N-P tests, we need to judge the validity of the same under *biased situations*. For example, if for a typical case, H_0 is biased with a higher probability to occur due to some application-specific reason, the numerical value of λ_0 will not be equal to 1.0. For example, consider the situation, wherein the global threshold is computed as $\lambda_0 = P_0 / P_1 \equiv P(H_0) / P(H_1) = 0.7/0.3$, i.e. $\lambda_0 > 1.0$. Similarly, the value of λ_0 will be less than 1.0, in case a situation gets biased with H_1. Thus, we surely need some other measurand for λ_0 that will be applicable for non-equally likely and/or biased hypothesis cases, as LLR and N-P are not suitable in such situations. The reason being in case of robotic gripping, we generally come across situations wherein only a 'point-object' or very small object is being grasped, leaving majority of the *taxels* free from getting exited. Hence, in such a situation, we need to bias the environment with the alternative hypothesis (H_1) in order to get fusion paradigms successfully. Likewise, biasing of hypothesis is a must for related situations, e.g. exciting the gripper sensor with a 'point-force'. Nonetheless, in situations wherein our main concern is

to disassociate the noise effects from the valid sensor data so that no erroneous reading can crop in during situations where no object is present physically, we need to bias the environment vis-à-vis optimization process with the null hypothesis (H_0).

b.   Situations where 'H_0' or 'H_1' are associated with penalty coefficients

Here the general expression for g*lobal threshold* (λ_0) is given as,

$$\lambda_0 = \frac{P(H_0)[C_{10} - C_{00}]}{P(H_1)[C_{01} - C_{11}]} \qquad (22)$$

where, 'C_{ij}' refers to the *cost* (penalty) of accepting 'H_i' when 'H_j' is true ($\forall$ i,j = 0,1).   Now, for a non-specific case, it goes very fine if we assume the values of the cost-coefficients, viz. numerically C_{10}, C_{00}, C_{01} & C_{11} to be 1,0,1 & 0 respectively. As a matter of fact, these are the standard values of the cost-coefficients used in majority of the fusion problems and hence the numerical value of the global threshold becomes 1.0. However, the *impended bias* situation does arise not only because of the probabilistic values of the null and alternative hypotheses but also the cost involved in accepting the incorrect hypothesis. For example, if a specific situation demands inherent bias to be incorporated, then, λ_0 will be a function of both P (H_k , $\forall$ k =0,1) and C_{ij} ($\forall$ i,j=0,1). In other words, we can certainly have non-zero values for C_{00} & C_{11} and non-unity values for C_{10} & C_{01}. In a way, this metric of evaluating global threshold is not unique and cannot be tackled by LLR or N-P method, when all 'C_{ij}' s are numerically different. In case of robotic grasp, we often need to use one or more penalty coefficients, as the exact model for λ_0 should account for instances like detecting point-force, grasping micro-objects, rectifying the readings from faulty taxels or correcting noise-levels of the taxels. In such situations, we need to use eqn.22, wherein the value of λ_0 will not be equal to unity and thereby that value of λ_0 will be unfit for LLR or N-P to process further.

Thus, we can observe that both of the well-accepted optimization tests, namely, LLR and N-P, do possess hindrances while tackling fusion problem pertaining to robotic gripping and these tests fail to address the divergent situations, such as biased or non-equally likely hypotheses and penalty factors. And, it is apparent that we need to have suitable metric for global threshold, which will be *dynamic* and able to handle such *biased hypotheses*. As a matter of fact, fusion problem in such situations should ideally be considered with *on-line observation* values and *posteriori processing* using suitable model. In that respect, our model (HEBTEM) proves to be a viable option in processing on-line sensory data from the *taxels* using the metric of dynamic threshold (λ_{Th}). The developed method is capable of tackling the situation of *selective biasing*, as the method is solely based on experimental observations and not any a-priori assumption.

3. Spotlight on the matrix sensor and jaw-gripper used for case-studies

3.1 Matrix sensor: case-study I for additive & multiplicative models

The prototype version of the sensory system (external dimension: 175 mm. x 160 mm. x 20 mm), used in the case study, has been optimally designed for a moderately spaced layout to house three categories of sensor units, viz. resistive ('R'), capacitive ('C') and Piezo ('P') cells in a matrix layout. The "R-cells", spaced in 4x4 array, have been designed in the form of small slender 'struts', with a rectangular cross-section (5 mm. x 4 mm., with a 2 mm. diameter blind hole inside).   A pair of strain gauges is pasted on the opposite walls of the struts. The capacitive cells, on the other hand, have been placed in a 5x5 matrix and these cells (15 mm. x

12 mm. x 5 mm.) have been designed taking into account the compliancy and overall sensitivity of the individual units, i.e. top & bottom plates and the dielectric layer. Figure 8 illustrates the schematic of the plan view of the of the matrix sensor used for the present study. A quasi-compliant protrusion pad atop protects these planar matrix-cells, having triangular / trapezoidal /spherical *serrations* embedded in it. Replaceable type pads are used, having triangular, trapezoidal or spherical serrations embedded. The protrusion pad has been designed in a way to make it quasi-compliant, shear stress-resistive and light-weighed. In the *assembled* version of the sensor system, a direct contact is being established between the struts and the serrations through slender pins, enabling the transmission of force(s) to the respective R-cells. Figure 9 schematically presents the internal disposition of the sensory assembly. 4 nos. PVDF sensors (P-cells, dimension: 25 mm. x 13 mm. x 205 µm) are mounted on the underneath of the protrusion (rubber) pad in a customized manner, so as to arrest micro-strains in both X & Y planes of the pad. The placement layout of the P-cells is illustrated in fig. 10.
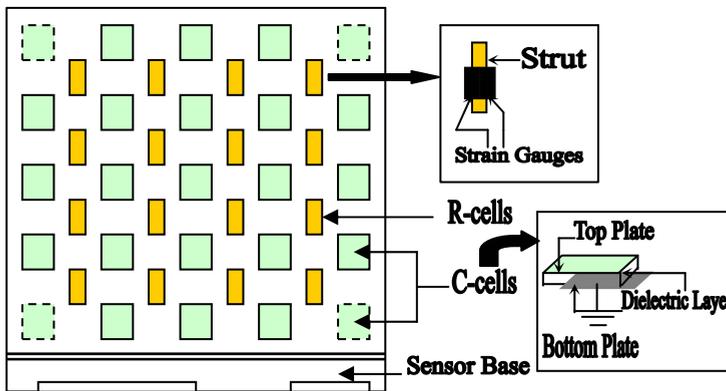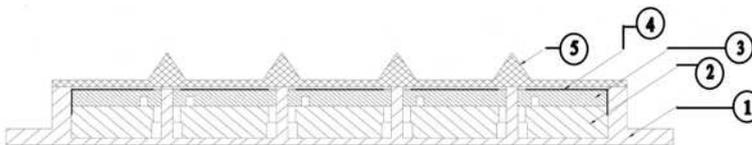

Fig. 8. Design metrics of the matrix sensor used in the case study I

Legends:
1: Base Plate   2: Bottom Support Plate [for the struts] 3: Top Guide Plate 4: Top Support Plate 5: Protrusion Pad

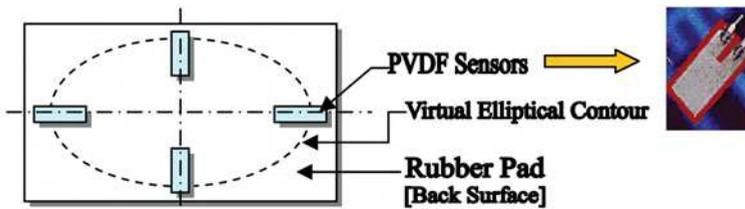Fig. 9. Sectional view of the sensor assembly in case study I

Fig. 10. Layout of the protrusion pad of the matrix sensor in case study I

The sensory system is being interfaced with a control circuitry, developed indigenously. The design is conceived as embedded system, with the provision for real-time processing of sensory signal. The control circuitry is conceptualized as optimally suited size, which necessarily compels minimum numbers of the measuring components for both R & C-cells. Sensory signals in analog form (mV) are being generated, as and when the cells are being *activated* through external force / *excitation.* The force-induced excitation gets manifested either in the form of *strains* generated in the strain gauges of the R-cells or by a change in capacitance in the C-cells, through the *instantaneous deformation* of the dielectric layer. The analog signals, so generated, are transferred to the control circuitry board (in the form of PCB) and are processed through stabilized circuits. The signals generated from the individual R & C-cells, then pass through micro-controller card and generate the final output signal. These *raw* output signals can be displayed over the VDUs (through serial communication with a PC or by using CRO) in real-time. The most appropriate fusion model is then superimposed on these raw data to get *unified* output.

3.2 Instrumented jaw gripper: case-study II for preferential selection model

The mechanical assembly of the planar parallel two-jaw robotic gripper, used in this case-study, comprises six major functional elements, namely, a] drive mechanism & associated drive train; b] motion transferring mechanism (through servomotor system); c] jaw assembly; d] drive for jaw movement; e] sensor assembly and related hardware and f] mounting structure (for assembling with the robot wrist). Nonetheless, the sensor system, augmented with the gripper body, includes the following four types, viz. a] *miniaturized load cell* for grip force evaluation [one per jaw, i.e. 2 in total]; b] *Infrared LED* for detection of object's presence /absence (three per jaw, i.e. 6 in total); c] *force sensor* for auxiliary measurement of grip-force (strain gauge, four in total, symmetrically placed over the moveable link) and d] *Thin-beam sensor* (TBS) for 'slip' measurement (five per jaw, i.e. 10 in total). Figure 11a presents a photographic view of the fabricated instrumented jaw gripper, with sensory interfaces (⊕) fitted inside the jaws, while the snapshots of the load cell (LC) & TBS (used for the slip sensor grid) are illustrated in fig. 11b,c respectively.
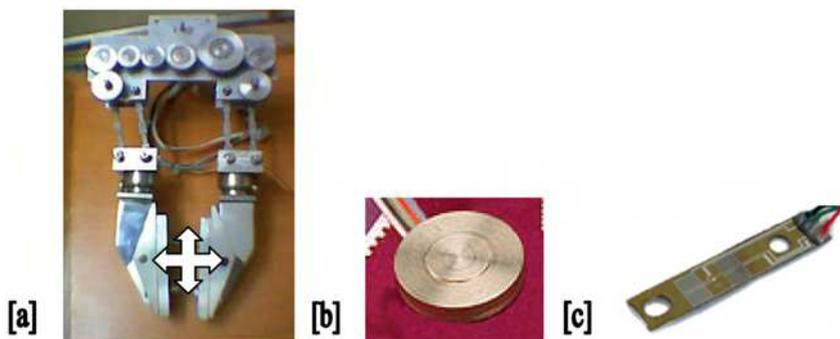

Fig. 11. Photographic view of [a] jaw gripper assembly [b] LC & [c] TBS used in case-study II

The fabricated hardware of the gripper system has suitable provision for easy mounting as a 'stand-alone' unit as well as while being interfaced with the wrist of the robotic manipulator. The drive system is through electrical d.c. servo-motor and the generated

rotational motion gets transmitted finally to the pair of jaws by means of gear-train and actuating system. The jaws are being activated through mechanical linkage-train, which follow semi-straight line path. The jaw assemblies are proportionate enough to house the sensory modules. The *sub-miniature* load cell has a cylindrical 'button' like shape in exterior (overall height: 3.2 mm), employing tiny metallic foil strain gauges with teflon insulated lead wires. On the other hand, thin-beam sensors employ specially developed instrumented strain gauge *assembly* (of 4 gauges), which is laminated to the *beam* to provide excellent stability vis-à-vis reliability.

4. Fusion model for evaluation of grip and slip force

The developed rule-bases are used to sense the external excitations on the gripper sensor or the jaw gripper (depending on the fusion model), operated remotely with an unknown loading. On assimilating raw sensory data, a *fusion model* is applied over in order to evaluate grip and slip force. Associated parameters, like slip velocity and slipped distance are also evaluated subsequently. Although the syntax of the fusion model is similar, it has been duly fine-tuned for a] additive & multiplicative rule-bases (i.e. for case-study I) and b] preferential selection rule-base (i.e. for case-study II), as detailed below.

4.1 Model for matrix sensor-based study

Here the model first evaluates tangential force on each of the affected taxels and afterwards, total tangential force or the *slip* force coming upon the sensor, based on the raw sensory signals. The gripping force is computed from the slip force and the allowable range of object loadings is decided thenafter. A straight-line interpolation is used to evaluate tangential forces on affected taxel(s), wherein the 'slope' ('m') and 'intercept' ('c') of the calibration line will jointly indicate the effect of other spurious force-components, largely non-tangential. The equation of the calibration line is given below,

$$y_j = m\,F_t^{\ k} + c \tag{23}$$

where, y_j: Raw output (in milli-volts) of the affected sensory cells due to object loading; F_t^k: Tangential force, generated on the $k^{th.}$ resistive cell .The total tangential force is evaluated by adding the individual forces vectorially. However, by virtue of the design of the matrix sensor, tangential forces on the cells are co-planar and parallel to one another. The exact number of R-cells affected will be ascertained from the object size, shape (i.e. convex hull profile) and weight. Hence, the gross tangential force is calculated numerically as,

$$Tot\,\vec{F}_t = \sum_{k=1}^{k=m} \vec{F}_t^{\ k} \equiv \left[\vec{F}_t^{\ (1,2)} + \vec{F}_t^{\ 3} + \ldots\ldots upto\,'m'\,terms \right] \tag{24}$$

Also,

$$\vec{F}_t^{\ (1,2)} = \left[\left(F_t^1\right)^2 + \left(F_t^2\right)^2 + 2\left(F_t^1\right)\left(F_t^2\right)Cos\alpha \right]^{1/2} \equiv \left(\left|F_t^1\right| + \left|F_t^2\right| \right) \tag{25}$$

where, $TotF_t$: Total tangential force on the sensor / gripper surface; F_t^k: Tangential force on the $k^{th.}$ cell; m: Total number of cells affected; $F_t^{(1,2)}$: The vectorial sum of the tangential

forces on the 1st. & 2nd. Cell; α: The inclusion angle between any two coplanar tangential force-vectors. The upper threshold of the gripping force ($F_g{}^{cal}$) vis-à-vis maximum allowable load (W) are evaluated as,

$$F_g{}^{cal} \leq \frac{\sum_{\forall k} F_t{}^j}{\mu}$$

(26a)

and

$$W = 2\mu F_g{}^{cal}$$

(26b)

where, '$F_t{}^j$' is the tangential force coming on the kth. resistive taxel at jth. time-instant & 'μ' is the coefficient of kinematic friction between sensor & the object surface. The inherent design of the matrix sensor generates tangential forces on the affected R-cells in case of gripping a large object, but, for objects with serrated contours, it will give rise to both tangential as well as normal reaction force on R- & C-cells respectively.

4.2 Model for jaw gripper-based study

In this case, the model relies on the characteristics of the external excitations on the jaw gripper. Based on the raw sensory signals from the thin-beam sensor grid (*TBS-cells*), the model first evaluates tangential force on each of the TBS-sensors and thenafter, total tangential force or the *slip force* coming upon the gripper. The gripping force is computed directly from the raw data of the load cells. A straight-line interpolation is used to evaluate tangential forces on affected TBS-taxel(s), wherein the 'slope' (m) and 'intercept' (c) jointly indicate the effect of other non-tangential spurious force-components. However, for load cell data, the calibration is straight-forward, with only a mapping factor (M). The equations of the calibration lines for the TBS and LC are given below,

$$y_j = m\,F_t{}^k + c$$

(27a)

$$Y_j = M\,F_g{}^k$$

(27b)

where, y_j: Raw output of the affected TBS-cells due to object loading; $F_t{}^k$: Tangential force, generated on the kth. TBS-cell; Y_j: Raw output from the LCs; $F_g{}^k$: Grip force, generated on the kth. LC. The total tangential force is evaluated by adding the individual forces vectorially. However, by virtue of the design of the gripper-sensor grid, tangential forces on the TBS-cells along one specific axis (e.g. X or Y) are co-planar and parallel to one another. The exact number of TBS-cells affected will be ascertained from the object size, shape (i.e. convex hull profile) and weight. The schematic layout of the TBS-grid in a single jaw is presented in fig. 12a (TBS-cells are numbered as #1,…,#5), while the overall sensory layout of the jaw and grasp force signature are shown in fig. 12b & 13c respectively.

Hence, the gross tangential force is calculated numerically as the vector-sum of 'X' & 'Y' components (i.e. $F_{t\text{-}x}$ & $F_{t\text{-}y}$) using the following model, viz.

$$Tot\,\vec{F}_{t-y} = \sum_{k=1}^{k=4} \vec{F}_{t-y}{}^k \equiv \left[\vec{F}_{t-y}^{(1,2)} + \vec{F}_{t-y}^{(3,4)} \right]$$

(28a)

where,

$$\overrightarrow{F}_{t-y}^{(1,2)} = \left[\left(F_{t-y}^{1}\right)^{2} + \left(F_{t-y}^{2}\right)^{2} + 2\left(F_{t-y}^{1}\right)\left(F_{t-y}^{2}\right)Cos\alpha\right]^{\frac{1}{2}} \equiv \left(\left|F_{t-y}^{1}\right| + \left|F_{t-y}^{2}\right|\right) \tag{28b}$$

and,

$$Tot\overrightarrow{F}_{t} \equiv \left[\overrightarrow{F_{t-x}} + \overrightarrow{F_{t-y}}\right] = \left[\left(TotF_{t-y}^{1}\right)^{2} + \left(F_{t-x}^{2}\right)^{2}\right]^{\frac{1}{2}} \tag{29}$$

where, $TotF_t$: Total tangential force on the sensor-grid / gripper surface; F_{t-y}^k: Tangential force on the kth TBS-cell along y-axis; $F_{t-y}^{(1,2)}$: The vectorial sum of the tangential forces on the 1st. & 2nd. Cell along y-axis; α: The inclusion angle between any two coplanar tangential force-vectors along y-axis; F_{t-x}: Tangential force on the TBS-cell along x-axis.
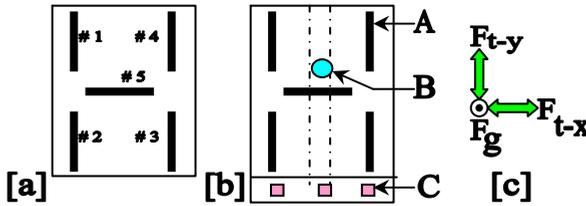
Index: A: TBS-cell; B: Load Cell; C: IR-cell; $F_{t-x,y}$: Tangential Force in x & y axes; F_g: Grip Force

Fig. 12. Layout of [a] TBS-sensor grid [b] overall sensory system & [c] grasp force signature

4.3 Overview of the software developed for case-study I
4.3.1 Schematic layout
The software, developed indigenously, has been customized for the statistical hypothesis testing of fused data evolved from the matrix sensor. It has a *core* module, like *backbone*, supported by four sub-modules, viz. [a] *Grip Force*, [b] *Slip Facets*, [c] *Planar Area* and [d] *Hypothesis Testing-cum-Optimality Check*. Each sub-module acts independently and provides quantitative output in terms of desired process parameters. The software is interlinked with 15 nos. *data files*, which either supply necessary input for the analytical computation or used for storing output data. The general layout of the software has been illustrated in fig. 13, highlighting functional dependencies between various sub-modules and data files.

The *beta* version of the software can incorporate a maximum of 200 sensor-cells, for which various categories of data (e.g. local co-ordinates, output response, noise threshold etc.) can be processed simultaneously. The entire code is framed considering [a] each of the resistive cell has got two R-taxels and [b] the number of rows and columns of R-cells are always one less than those of the C-cells.

The software also provides an interactive session as *front-end*, wherein user can feed design data relevant for the statistical analysis. In general, these user-input data are of two types, one related to the physical hardware of the sensor and the other one incorporates variables needed for fusion analysis. The former group notes the information, such as number of columns and rows in C & R-cells, pitch distance of the C- & R-taxels and evaluates data like

total number of sensor-cells (taxels) and total number of data points in the matrix sensor as output. Similarly, the latter group takes the numerical values for ξ, k, $P(H_1)$, $P(H_0)$ and the delay (in seconds) before the next output, as desired by the user.
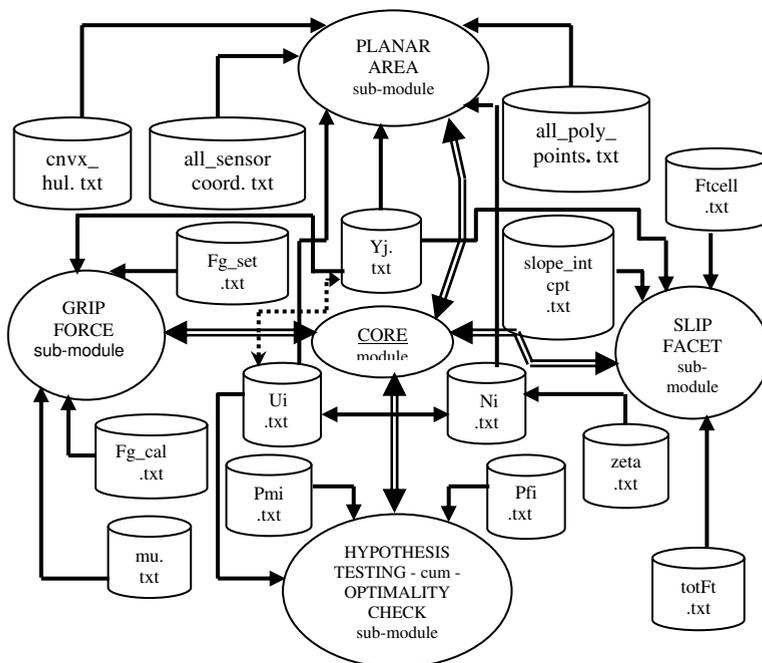

Fig. 13. Organizational layout of the developed software using fusion models

It may be noted that the sub-modules concerning evaluation of grip force, slip force and planar area of the object being grasped work coherently to certain extent and mutually share a group of data files (e.g. y_j.txt). However, the optimality check sub-module needs different inputs, such as data files for 'probability of false alarm' (P_{fi}.txt) and 'probability of miss' (P_{mi}.txt), alongwith other files. 'P_{fi}.txt' and 'P_{mi}.txt' are required only for analyzing the case-study while using LLR or N-P test. These are not needed for our method, viz. HEBTEM.

4.3.2 Sub-modules for the evaluation of grip force, slip facets and planar area

For interim processing of grasp and slip force, the program is able to tackle a maximum of 150 data-points at a time, of which, a set of 100 points go critical mainly for the evaluation of planar area of the object grasped. The program code uses dummy variable in order to indicate the number of data points stored in a file and also keep a record of respective Cartesian co-ordinates. This set of *data map*, viz. taxel number and its co-ordinates, has been used for the computation of planar area of the object being grasped.

The program takes the 'y_j' values from a text file, wherein 'y_j' values are put in the order of increasing value of the 'ordinate' (i.e. 'y' co-ordinate) and the points having same 'y' are stored in the order of increasing 'x'. It takes the noise data, viz. 'N_i', in a similar manner from another text file. The program performs a confirmatory check to ascertain the correctness of the number of data-point entries in the corresponding files. It then calls for the

value(s) of the noise threshold (i.e. ξ, as per eqns. 3 & 4), both for the R- and C-cells. The program then evaluates $\{u_i\}$ matrix as per the model, described earlier. It stores 'u_i' values $[\forall u_i, \in (-1, 1)]$ in a text file, in the same way as 'y_j'. The program then decides the presence or absence of the object by calculating 'U_G' as per the fusion rules. Using the calibration data of the R-cells (analog signal in mV vs. force applied), the code calculates the total tangential force ($totF_t$) acting on the sensor-pad and controls the gripping force. Essentially, the program takes the calibration values from a text file (namely, 'slope_intcpt.txt'), having a pair of entries ('slope' & 'intercept') per R-cell alongwith 'y_j' values. It then calculates the instantaneous tangential force on each active R-taxel as,

$$F_t^j[i] = \frac{\left(y_j[i] - incpt[i]\right)}{slope[i]} \tag{30}$$

where, $F_t^j[i]$: Instantaneous tangential force for i^{th} resistive taxel at j^{th} time-instant; $y_j[i]$: Sensory reading (in mv.) for i^{th} resistive taxel at j^{th} time-instant; *incpt [i]*: Intercept value of the calibration line for i^{th} resistive taxel; *slope[i]*: Slope value of the calibration line for i^{th} resistive taxel. Once the numerical value of the tangential force at each R-taxel at a given time-instant is evaluated, the program finds out the total tangential force generated vis-à-vis the required gripping force by using the model (viz. eqns. 24 & 25). It may be noted that 'slope_intcpt.txt' file must have dummy entries corresponding to C-cells. Ideally, the 'slope' of the C-cells should be zero, signifying infinite tangential force (to be applied) on that C-cell. This is logical, as C-cells are comparatively more sensitive towards normal force in the prototype design.

The software stores the Cartesian co-ordinates of all the taxels in a text file (all_sensor_coord.txt) in the order of increasing 'y' (if two or more taxels have got same ordinate, then it is put in the order of increasing 'x'). As per the design, R-cells are assumed to be at the center of the *rectangle* formed by four C-cells and their co-ordinates are being evaluated accordingly. The next part takes the 'u_i' values from 'u_i.txt' and coordinates all the points from 'all_sensr_coord.txt' and finds those points only which are sending recognizable signal (above the threshold, as described by 'zeta.txt') and prints those points to 'all_poly_points.txt'. The module then examines the points that are on the *convex hull* from the previous file and puts those in 'cnvx_hul.txt' in either clockwise or counter-clockwise manner. The planar area of the polygon, determined by the convex hull so formed, is calculated thereafter.

4.3.3 Hypothesis testing -cum- optimality check sub-module

This module checks the presence or absence of the object in the gripper through the testing of the hypothesis using the fusion rule-bases described a-priori. After hypothesis testing, the program evaluates the value of the global threshold (λ_0) using HEBTEM as well as *Log-Likelihood Ratio* (LLR) and *Neyman-Pearson* (N-P) tests. The LLR & N-P tests are incorporated in the module so as to make a comparative judgment between the existing methods and our method. Now, in order to evaluate the global threshold using HEBTEM ($\lambda_{Th.}$), we will use eqn. 16 or 17. Then after, the final decision on the selection of hypothesis will be made by evaluating the numerical value of 'U_G', as described in section 2.2.2. On the contrary, the numerical value of the global threshold by LLR test is evaluated as per the standard formulae, viz.

$$\lambda_{\text{threshold}}^{\text{LLR}}(U) = \log \frac{P(H_1 | U)}{P(H_0 | U)} = \log \frac{P_1}{P_0} + \sum_{s+} \log \frac{1 - P_M^i}{P_F^i} + \sum_{s-} \log \frac{P_M^i}{1 - P_F^i} \qquad (31)$$

where, U: The *global* event that data is generated out of the sensor-cells; P_1: The un-biased estimate of $P(H_1)$; P_0: The un-biased estimate of $P(H_0)$; P_M^i : The probability of miss for the $i^{th.}$ sensor-cell; P_F^i: The probability of false alarm for the $i^{th.}$ sensor-cell; 'S+':The set of all 'i', such that $\{u_i = +1\}$ and 'S-':The set corresponding to $\{u_i = -1\}$. The final selection of hypothesis is being governed by the numerical value obtained for $\lambda_{\text{threshold}}^{\text{LLR}}$, namely, if $\lambda_{\text{threshold}}^{\text{LLR}} > 0$ then accept 'H_1'. Likewise, the global threshold by N-P test is computed as,

$$\lambda_{\text{threshold}}^{\text{N-P}}(U) = \frac{P(U | H_1)}{P(U | H_0)} = \prod_{i=1}^{i=n} \left(\frac{1 - P_M^i}{P_F^i} \right)^{u_i} \left(\frac{P_M^i}{1 - P_F^i} \right)^{1-u_i} \equiv \prod_{s+} \left(\frac{1 - P_M^i}{P_F^i} \right) \prod_{s-} \left(\frac{P_M^i}{1 - P_F^i} \right) \qquad (32)$$

where all the legends bear the same definition, as of eqn. 31. The final selection of the hypothesis is made through the following proposition, viz. if $\lambda_{\text{threshold}}^{\text{N-P}}(U) > \lambda_{\text{threshold}}$, then '$H_1$' is true and if $\lambda_{\text{threshold}}^{\text{N-P}}(U) < \lambda_{\text{threshold}}$ then 'H_0' is true. Here, '$\lambda_{\text{threshold}}$' signifies the threshold under un-biased condition of the hypotheses, i.e. the value of '$\lambda_{\text{threshold}}$' is 1.0.

## 5. Synthesis of the model under various grasp postures

One of the salient aspects of the developed model is its ready applicability in practical situations, pertaining to different grasp postures. Apart from using HEBTEM on a stand-alone tactile sensor, we need to explore its functional utility while interfaced with a robotic gripper. In this section, we will examine three major types of contact between the object and the gripper-jaw and draw an analogy between the contact semantics of those grasp-postures and the HEBTEM attributes. We will design analytical metric to classify the contact-types and retrofitting the rule-bases of HEBTEM thereon.

5.1 Jaw-based gripping re-visited

We will discuss the case with reference to a planar parallel two-jaw robotic gripper, which is capable to gripping objects, as restricted by its shape, size and payload threshold. A pair of matrix sensors (refer section 3, fig. 8) is mounted on the jaw surfaces at suitable location and soft rubber padding is provided over it. Figure 14 schematically shows the disposition of this sensor-instrumented jaw gripper, in course of grasping an object. The figure also illustrates the contact metrics between the jaw and object, highlighting on the *asperity contact*. It may be mentioned that it is the geometry of the contact between the asperities of both the object and the jaw surface that defines the type of contact, prior to a stable grasp.
We shall now examine the three major types of contacts, prevailing in the domain of planar grasp. We may categorize these as: a] *Point Contact (without friction)*; b] *Point Contact (with friction)* and c] *Soft Finger Contact*. However, this classification is in turn dependent on the *relative nature* of the jaw and object surface, e.g. we can have soft jaw vs. hard jaw vis-à-vis soft object vs. hard object. Thus, theoretically speaking, we can get four combinations in total, namely, I] soft jaw_ soft object; II] soft jaw_ hard object[1]; III] hard jaw_ soft object and IV] hard jaw_ hard object. Now considering various feasible combinations between the

---

[1] A combination of soft jaw and hard object is impractical for real-life use.
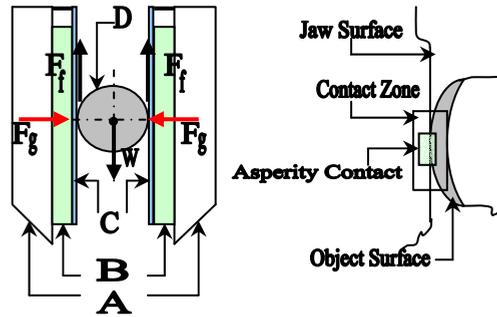
Legends: **A:** Gripper Jaws; **B:** Matrix Sensors; **C:** Rubber Pads; **D:** Object Gripped; **W:** Weight of the Object; $\mathbf{F_g}$**:** Grip Force; $\mathbf{F_f}$**:** Friction Force.

Fig. 14. Disposition of the grasp condition and contact for a planar two-jaw robotic gripper

nature of jaw and object, we can define a parameter, which will measure the *conjugate softness* of the *jaw-object pair* in a relative scale. We will term this parameter as *relative softness index* (RSI) and will be defined as,

$$RSI = \frac{Softness_{Object}}{Softness_{Jaw}} - 1 \equiv \frac{1/H_O}{1/H_J} - 1 = \frac{H_J}{H_O} - 1 \qquad (33)$$

where, 'H_J' and 'H_O' represent the hardness values for the jaw and object respectively, measured through an uniform *Rockwell* Scale. It may be mentioned here that in a dynamic condition, governed by the Coulomb's laws of friction, the variation of the three groups of contact is essentially dependant on the value of RSI. For example, a very low numerical value of RSI will target towards point contact (without friction) while a high value of RSI hints for a soft finger contact. Obviously the zone for point contact (with friction) lies in-between these two extremities, with a fairly large range. Figure 15 illustrates an idealistic distribution of the contact zones with respect to the variation of relative softness index. It also highlights a case of *Locked Contact*, with RSI=0, where there is no movement even between the asperities of both object and jaw.
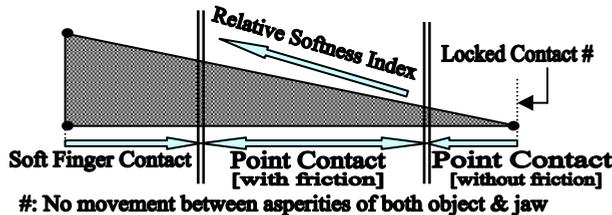

Fig. 15. Schematic view of the distribution of contact zones as contrasted with RSI

5.2 Mapping of contact criteria to HEBTEM rule-bases

The mechanics of contact between the object and the jaw starts zooming in once the object is grasped between the jaws of the gripper. The taxels of the matrix sensor get excited by the external loading as a consequence of the contact. However, we need to have a thorough

mapping between different contact-types and the level of taxel-excitation in order to arrive at a decision regarding the nature of the object. Once we get the data regarding the excited taxels, alongwith their location on the sensor, we can use HEBTEM for the optimality test and can infer about the presence / absence of the object in the gripper-zone. Keeping in mind the basics of the three contact-types referred here, qualitatively we can infer the nature of taxel-excitation. For example, the situation of frictionless point contact is equivalent to the case of excitation of the taxels by 'point-force', while point contact with friction is analogous to impingement by small or very tiny objects and soft finger contact is mapped through an external loading by a comparatively large object.

With this qualitative paradigm, we will now introduce the concept of *friction surface* and *friction plane*, in relation to the taxel geometry of the matrix sensor. Enveloping all the excited taxels of the matrix sensor generates a *friction surface* and the corresponding projection in the 2D plane is denoted as the *friction plane*. As soon as a grasp takes place the contact-type between the jaw-object interface is frozen and the excitation of the taxels begins thereof. The extent of such excitation is imaged on the friction surface and its effect is ascertained by measuring the area of the friction plane. Figure 16 pictorially explains this mapping scenario, wherein all three types of contact criteria have been studied through a] physical view at the gripper; b] spatial view at the matrix sensor in order to represent 3D friction surface and c] planar view of the friction plane, as generated.
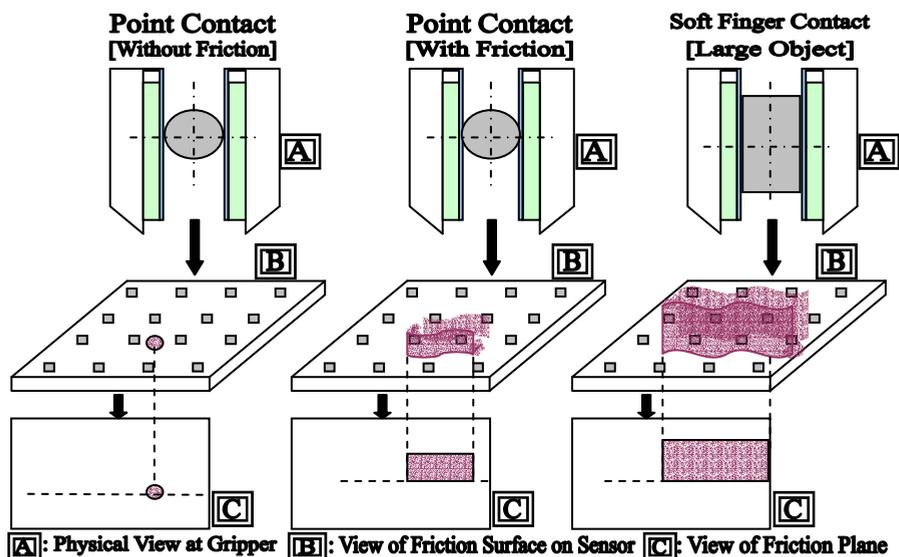

Fig. 16. Schematic view of the mapping of contact criteria during grasping

We propose two methods in order to map the contact-types with the equivalent object description, in terms of taxels. These are: 1] *Taxel_Count* (t_c) and 2] *Friction_Plane_Area_Count* (fp_c). The computations of the two methods are as follows,

$$t_c = \frac{N_{affected}}{N_{total}}$$
(34a)

and

$$fp_c = \frac{\Delta_{friction\_plane}}{\Delta_{total}}$$ (34b)

where, $N_{afftected}$: Number of taxels excited by the grasp, i.e. the contact between the object and the jaw; N_{total}: Total number of taxels present in the sensor; $\Delta_{friction\_plane}$: Area of the *friction_plane* and Δ_{total}: Total area of the taxels, i.e. the planar area of the sensor. It is apparent that both of these methods essentially tells us the comparative range of the taxels affected, which will be used finally in judging the hypothesis by knowing the threshold for HEBTEM ($\lambda_{Th.}$) a-priori. Table 1 describes the mapping index between the three groups of contact-types and the corresponding signature in using fusion logic and HEBTEM.

Contact Type	Equivalent Object Nomenclature	Taxel Signatures & Analytical Limits
Point Contact [Without Friction]	"Point-force"	Taxel Signature: "*Least*" Limits: $0.01 \leq \{t_c, fp_c\} \leq 0.02$
Point Contact [With Friction]	Small / Very Tiny Object	Taxel Signature: "*Minimum*" Limits: $0.01 \leq \{t_c, fp_c\} \leq 0.1$
Soft Finger Contact	Bigger Object	Taxel Signature: "*Moderate to High*" Limits: $0.1 \leq \{t_c, fp_c\} \leq 1$

Table 1. Mapping index for different contact-types during jaw-based grasp

Thus, we get a working thumb-rule for distinguishing different contact-types mathematically, by evaluating *taxel_count* and/or *friction_plane_area_count*. Once the numerical values for 't_c' and 'fp_c' are obtained, those can be mapped (as per Table 1) and the contact-type vis-à-vis equivalent object nomenclature, as prevailed in the specific grasp action, is to be determined. Also, since *txael_count* is known numerically, we get the exact number of taxels affected by the loading, which will give us $\{u_i\}$ matrix for the sensor and the gripper in action. The subsequent procedure will follow thereon, i.e. use of rule-bases and confidence level and finally, we can judge the hypothesis as per HEBTEM, as stated earlier. It may be stated that although identical fusion rules are applied in all the three contact situations, different values of λ_{Th} may be adopted based on the equivalent object nomenclature.

6. Simulation studies

6.1 Perspective

The proposed hypothesis, HEBTEM has been tested thoroughly using simulated results, prior to real-life experimentation on the matrix sensor & jaw gripper respectively. Nonetheless, the simulated sensor-data have been assumed to represent the basic functioning of the sensor & gripper, only difference being that those are not real-time data. Considering the case-study for matrix sensor, We analyze HEBTEM vis-à-vis traditional optimization techniques (namely, LLR and N-P tests) for checking the condition of presence / absence of object, aided by requisite matrices, viz. 'P_{fi}' (Probability of False Alarm), 'P_{mi}' (Probability of miss), 'Y_i' (raw sensor output) and 'N_i' (sensor noise). Each matrix is

composed of data, arranged row-wise in increasing order[2], pertaining to the *active taxels* of the matrix sensor. However, four C-cells, located at the four corners of the sensor-matrix (marked with dashed-line border in fig. 8) are not included in the data fusion algorithm. This has been done deliberately as none of the objects tried under real-life testing are covering up those corner C-cells. Hence, in a way we are only considering 21 *C-cells*, 32 *R-cells* and 4 *P-cells* in action.

6.2 Simulation results

We are having the following four matrices, namely, 'P_{fi}', 'P_{mi}', 'Y_i' and 'N_i' as input, each of which has got 57 readings, pertaining to 57 taxels in action.
Probability Matrix of *False Alarm* (P_{fi}):

$$\begin{bmatrix} 0.0005 & 0.0023 & 0.0010 & 0.0002 & 0.0002 & 0.0004 & 0.0005 & 0.0013 & 0.0006 & 0.0004 & 0.0066 & 0.0021 & 0.0005 & 0.0033 & 0.0005 & 0.0034 & 0.0002 & 0.0005 & 0.0033 \\ 0.0056 & 0.0052 & 0.0056 & 0.0032 & 0.0064 & 0.0013 & 0.0024 & 0.0075 & 0.0013 & 0.0044 & 0.0013 & 0.0035 & 0.0046 & 0.0003 & 0.0076 & 0.0021 & 0.0005 & 0.0033 & 0.0005 \\ 0.0034 & 0.0002 & 0.0005 & 0.0033 & 0.0056 & 0.0052 & 0.0050 & 0.0020 & 0.0064 & 0.0013 & 0.0024 & 0.0075 & 0.0013 & 0.0044 & 0.0013 & 0.0035 & 0.0046 & 0.0003 & 0.0076 \end{bmatrix}$$

Probability Matrix of *Miss* (P_{mi}):

$$\begin{bmatrix} 0.0015 & 0.0022 & 0.0030 & 0.0052 & 0.0062 & 0.0074 & 0.0085 & 0.0093 & 0.0076 & 0.0054 & 0.0036 & 0.0023 & 0.0004 & 0.0005 & 0.0006 & 0.0008 & 0.0032 & 0.0025 & 0.0013 \\ 0.0036 & 0.0052 & 0.0006 & 0.0007 & 0.0008 & 0.0009 & 0.0054 & 0.0008 & 0.0006 & 0.0043 & 0.0023 & 0.0055 & 0.0066 & 0.0043 & 0.0006 & 0.0023 & 0.0004 & 0.0005 & 0.0006 \\ 0.0008 & 0.0032 & 0.0025 & 0.0013 & 0.0036 & 0.0052 & 0.0006 & 0.0007 & 0.0008 & 0.0009 & 0.0054 & 0.0008 & 0.0006 & 0.0043 & 0.0023 & 0.0055 & 0.0066 & 0.0043 & 0.0006 \end{bmatrix}$$

The off-line data matrix for the raw sensory output (in milli-volts) (Y_i):

$$\begin{bmatrix} 2.3 & 7.8 & 0.6 & 0.8 & 15.6 & 5.8 & 2.4 & 18.0 & 4.3 & 5.5 & 4.2 & 0.5 & 3.7 & 2.7 & 5.1 & 5.4 & 8.8 & 19.3 & 14.6 \\ 11.7 & 7.8 & 3.6 & 8.5 & 4.4 & 5.69 & 5.5 & 2.6 & 6.4 & 8.8 & 4.88 & 17.0 & 2.9 & 13.4 & 9.0 & 5.6 & 6.5 & 7.5 & 8.5 \\ 9.5 & 7.5 & 6.4 & 5.3 & 4.3 & 3.5 & 2.6 & 2.6 & 4.4 & 4.5 & 5.6 & 6.7 & 7.8 & 8.4 & 9.6 & 0.4 & 9.5 & 4.6 & 6.7 \end{bmatrix}$$

The system noise (in milli-volts.) (N_i):

$$\begin{bmatrix} (0.1) & (0) & (0) & (1) & (0.8) & (1) & (1) & (1) & (0) & (0) & (0.9) & (1) & (1) & (0) & (0) & (0.5) & (0.4) & (1) & (1) \\ (0.6) & (1) & (0) & (0) & (1.2) & (1) & (1) & (1.3) & (0) & (0.3) & (0.7) & (1) & (0) & (1) & (1) & (0) & (0) & (0) & (0) \\ (0) & (1) & (1) & (1) & (1) & (0) & (0) & (1) & (1) & (0) & (0) & (1) & (1) & (0) & (1) & (0) & (1) & (0) & (0) \end{bmatrix}$$

Now, using these simulated sensor-data, $\{u_i\}$ matrix $[u_i \in (-1,1)]$ computed as,

$$\begin{bmatrix} -1 & -1 & -1 & -1 & 1 & -1 & -1 & 1 & -1 & -1 & -1 & -1 & -1 & -1 & -1 & -1 & -1 & 1 & 1 \\ 1 & -1 & -1 & -1 & -1 & -1 & -1 & -1 & -1 & -1 & -1 & 1 & -1 & 1 & -1 & -1 & -1 & -1 & -1 \\ -1 & -1 & -1 & -1 & -1 & -1 & -1 & -1 & -1 & -1 & -1 & -1 & -1 & -1 & -1 & -1 & -1 & -1 & -1 \end{bmatrix}$$

Based on the simulated observation values of *taxels*, we have the final value for the global threshold ($\lambda_{threshold}^{LLR}$) as –135.9376, which signifies a strong case for rejecting H_1, inferring no object is present within the graspable zone of the gripper. In fact, this evaluation is strongly influenced by the number of sensor-cells having $\{u_i = 1\}$, which, in this case is only seven (vide cell nos. 5, 8, 18, 19, 20, 31 & 33). Hence, by this test we are likely to exclude those options wherein a relatively tiny object is being gripped by the gripper or for that reason, a point-object / force is impinging on the sensor / gripper body.
Nonetheless, the pre-conceived value for the global threshold under LLR method (which is 1.0, as stated in section 2.2.3.4) also plays a deciding role in this regard. Even if we assume a non-unity value for global threshold, we need to check the values of the cost-coefficients,

---

[2] Two taxels positioned at one R-cell, giving 41 different locations for a total of 61 taxels.

such that they follow at least one of the conditions, viz. [a] $C_{10} > C_{00}$ & $C_{01} > C_{11}$; [b] $C_{10} < C_{00}$ & $C_{01} < C_{11}$. In all other cases, the test will fail, which is certainly a major bottleneck of the method itself. Moreover, the tests will lead to undefined zones of hypothesis, when the value of $\lambda_{threshold}^{LLR}$ will be equal to zero or other non-zero value.

That's why, although computationally simpler, this test lacks in handling the specific situations concerning very small object, point-force, instant impulse etc. and also the undefined cases.

For N-P test, we get the final value for the $\lambda_{threshold}^{N-P}$ as $26.19898 \times 10^{-143}$, which again signifies a strong case for rejecting H_1 (assuming $\lambda_{threshold}$ to be 1.0 in an un-biased case). However, this test also fails to identify the hypothesis in case the numerical value of $\lambda_{threshold}^{N-P}$ becomes exactly equal to $\lambda_{threshold}$. As argued earlier, this test too fails to satisfy the varied situations of robotic grasping involving miniaturized objects and point-force.

Thus, we have found from the simulation results that although traditional optimization methods, such as LLR & N-P, may be used for *larger objects* but there is no guarantee those would give correct inference for *miniaturized objects* or *'point-objects'*. As a matter of fact, fusion problem in such situations should ideally be considered with on-line observation values and posteriori processing using suitable model. In that respect, our model proves to be a viable option.

6.3 Optimized solution using HEBTEM

Evaluation of global (dynamic) threshold ($\lambda_{Th.}$) is relatively easier using HEBTEM, which also clearly demarcates the acceptance/rejection regions of 'H_1'. For example, considering multiplicative model of fusion, if 83% Type II error has been set as the accepted limit (i.e. $\beta = 0.83$), then, in the present case with n=57, we get the numerical value for $\lambda_{Th.}$ as 1.663×10^{-20} (=$e^{-45.543}$, refer eqn. 16). Similarly, in additive model of fusion, we get the value for $\lambda_{Th.}$ with n = 57 as ± 49.753 (refer eqn. 17), respectively against 3% Type I error (i.e. $\alpha = 0.03$) and 47.3% Type I error (i.e. $\alpha = 0.473$). Once the dynamic threshold is evaluated by either of the fusion models, the next phase what HEBTEM takes care is determination of the following facets, viz. [a] inference about the presence or absence of object /point-force in the vicinity of the gripper; [b] evaluation of the grip and slip force and [c] determination of the planar area of the object being grasped and/or impinged upon, as explined in detail below.

6.3.1 Inference about presence of object using fusion logics

Considering the simulated situation, i.e. wherein seven cells are giving acceptable signal (vide cell nos. 5, 8, 18, 19, 20, 31 & 33), U_G has been computed. For example, using additive model, U_G becomes – 43 (vide eqn. 6) and likewise multiplicative model gives the value of U_G as 2.11513×10^{-19} (=e^{-43}, vide eqn. 5). Now, the dynamic threshold obtained for additive model being – 49.753 (which is less than – 43, i.e. the value of U_G)[3], the presence of object is confirmed. Also, the value of dynamic threshold for multiplicative model being 1.663×10^{-20} (which is less than 2.11513×10^{-19}, i.e. the value of U_G), the presence of object is inferred. It is interesting to note that the value of $P(H_1)$, corresponding to U_G in additive and multiplicative model comes out to be 0.124835 and ≈ 0.003 respectively (using the curve in figs. 2a & 4). Hence, although the presence of object is confirmed, yet different fusion logic infers the situation with different *levels of conformity*, viz. the value of $P(H_1)$.

---

[3] We consider left hand side of the curve shown in fig. 4, since the sign of U_G is negative.

6.2.3.2 *Evaluation of Slip and Grip Force*

We consider the following data for 'slope' and 'intercept', as required for the calibration of tangential force. These are represented in conjugate inside the bracket ( ), the first term being the 'slope' and the second term is the 'intercept' (i.e. 'm' and 'c' respectively, as per eqn. 23). The 'slope' & 'intercept' matrix:

$$\begin{bmatrix} (0,6) & (0,6) & (0,6) & (0,3) & (8,0) & (7,1) & (9,2) & (5,3) & (6,1) & (3,1) & (9,8) & (9,1) & (9,4) & (0,2) & (6,3) & (2,4) & (3,7) & (4,2) & (3,4) \\ (2,4) & (2,1) & (3,6) & (3,0) & (4,7) & (3,4) & (8,2) & (9,2) & (7,3) & (4,2) & (3,3) & (4,2) & (0,5) & (6,1) & (5,1) & (5,1) & (4,4) & (3,2) & (6,3) \\ (2,4) & (3,7) & (2,1) & (4,2) & (3,4) & (0,4) & (3,6) & (2,0) & (4,7) & (5,4) & (8,2) & (9,2) & (7,3) & (4,2) & (3,3) & (0,5) & (0,2) & (0,1) & (0,1) \end{bmatrix}$$

With the 'm' & 'c' values for the calibration of tangential (slip) force are known a-priori, the tangential forces on the affected taxels are computed using eqns.23 & 25. The calculated values of 'F_t' for taxel no. 5, 8, 18, 19, 20, 31 & 33 are 1.95, 3.00, 4.325, 3.5333, 3.85, 3.75 & 2.06667 units respectively and total tangential/slip force is 22.475 units. The upper threshold for grip force can thus be evaluated knowing the value of coefficient of dynamic friction (eqn. 26a). Similarly, maximum limit of allowable loading may be ascertained from eqn. 26b.

6.2.3.3 *Determination of planar area of the graspable object*

The size of the object (which is being gripped remotely and impinging on the tactile sensor matrix) is determined using the raw sensor data. After getting filtered for the sensor noise, these data are used to ascertain the location of the taxels and subsequently, Cartesian co-ordinates of those taxels are recorded. Figure 17 shows a typical case wherein 'n' taxels are registered for giving {u_i = +1}.
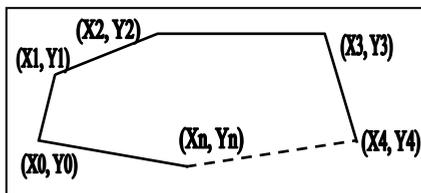

Fig. 17. Convex hull generated from the readings of the taxels of the matrix sensor

The planar area (A) of the convex hull generated thereon is computed as,

$$A = \frac{1}{2} \sum_{i=0}^{i=N-1} \left(X_i Y_{i+1} - X_{i+1} Y_i \right) \tag{35}$$

The associated program code first finds the co-ordinates of those taxels giving *recognizable* signals. Now, a *point* (i.e. taxel location) is selected having maximum Y-co-ordinate, which will always lie on the convex hull. Then it checks every double combination of the remaining points with that point, selected a-priori to find the maximum included angle. Thus the 'second' such point will be selected as a point on the convex hull.

Figure 18 illustrates the schematics of the layout of the 57 taxels of the matrix sensor and their nomenclature, in order to develop a one-to-one mapping between the taxel number and its co-ordinates. In general, 'T_x' denotes the $x^{th.}$ taxel ($\forall x$ =1,2,………,57), but it is not indicative of the *location* of that taxel precisely. In contrast, '$T_{j,k}$' denotes $j^{th.}$ & $k^{th.}$ taxels placed at same location. Hence in the pictorial layout 'T_x' represents a C-cell, '$||T_y||$' represents a P-cell and '$T_{j,k}$' represents a R-cell (x,y≠j,k). This nomenclature is essential. The

legend, '*d*' (dummy) signifies the four corner locations of the C-cells, which are not participating in the fusion algorithm.

$$
\left\|
\begin{array}{ccccccc}
d & T54 & T55 & \|T57\| & T56 & & d \\
 & T46,47 & T48,49 & T50,51 & T52,53 & \\
T41 & T42 & T43 & T44 & & T45 \\
\|T31\| & T32,33 & T34,35 & T36,37 & T38,39 & \|T40\| \\
T26 & T27 & T28 & T29 & & T30 \\
 & T18,19 & T20,21 & T22,23 & T24,25 & \\
T13 & T14 & T15 & T16 & & T17 \\
 & T5,6 & T7,8 & T9,10 & T11,12 & \\
d & T2 & T3 & \|T1\| & T4 & & d
\end{array}
\right\|
$$

Fig. 18. Nomenclature of taxels of the matrix sensor for simulation

The planar co-ordinates of the taxels have been arrived at after considering the locational matrix of the 41 taxels (21 C-cells, 16 R-cells & 4 P-cells), assigned proportionately with the design and dimensions of the prototype sensor, as detailed out below.

$$
\left[
\begin{array}{ccccccc}
(1,104) & (21,104) & (41,104) & \|(51,107)\| & (61,104) & & (81,104) \\
 & (11,91.5) & (31,91.5) & (51,91.5) & (71,91.5) & \\
(1,79) & (21,79) & (41,79) & (61,79) & & (81,79) \\
\|(1,66.5)\| & (11,66.5) & (31,66.5) & (51,66.5) & (71,66.5) & \|(82,66.5)\| \\
(1,54) & (21,54) & (41,54) & (61,54) & & (81,54) \\
 & (11,41.5) & (31,41.5) & (51,41.5) & (71,41.5) & \\
(1,29) & (21,29) & (41,29) & (61,29) & & (81,29) \\
 & (11,16.5) & (31,16.5) & (51,16.5) & (71,16.5) & \\
(1,4) & (21,4) & (41,4) & \|(51,1)\| & (61,4) & & (81,4)
\end{array}
\right]
$$

For example, the off-line data for the taxel observations (X_i), noise (N_i) and subsequently $\{u_i\}$ lead to the taxels at the locations (11,16.5), (31,16.5), (11,41.5), (11,41.5), (31,41.5), (1,66.5) & (11,66.5) to be the points on the desired polygon. These locations correspond to the taxel nos. 5, 8, 18, 19, 20, 31 & 33. The convex hull, so generated, will have its planar area of 625 sq. units, considering five major vertices.

7. Case studies and experimentation

HEBTEM has been tested using field-results of the experimentation on the matrix sensor as well as sensor-augmented jaw gripper. Through the field-trials, global threshold was evaluated, alongwith other model-specific parameters. We will present these findlings below.

7.1 Testing with matrix sensor

The sensor has been calibrated with a series of *object*, having pre-assigned contour but varying weight in real-time. The pictorial representation of the object, used for calibration as well as final testings, is shown in fig. 19.
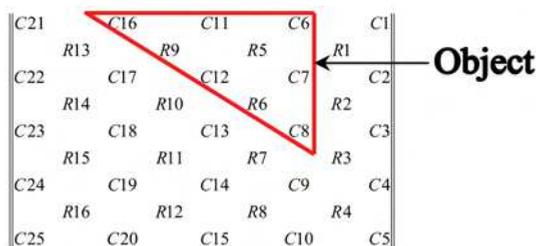
Fig. 19. Pictorial view of the test scheme with the objects for case-study I

The sensor is loaded with the *object-sets*, having weights ranging from 0.9 kg. to 4.3 kg. However, due to serrated skin, it is not possible to have simultaneous excitation of the R & C-cells. As a matter of fact, only R-cells, namely, R5, R6 & R9 are affected in this test (refer fig. 19). The calibration of the respective struts reveals the regression equations (considering straight line trend), which were used to evaluate tangential force on each R-cell numerically. Based on the testing, the calibration equations for the struts are determined as follows,

$$\begin{bmatrix} Y\_R5 \\ Y\_R6 \\ Y-R9 \end{bmatrix} = \begin{bmatrix} 0.1661 \\ 0.307 \\ 0.3185 \end{bmatrix} \{F\_T\} - \begin{bmatrix} 0.0155 \\ 0.0163 \\ 0.0133 \end{bmatrix} \qquad (36)$$
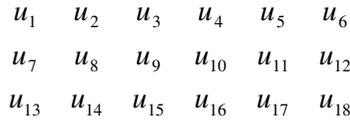
where, $[Y\_Rj]$, $\forall j=5,6,9$ signifies the sensory output (in mV) from the respective R-cells, against the loadings (manifested in tangential force, '*F_T*').

The matrix sensor was then tested for *unknown* loadings (using objects having same contour as used in the calibration of the three R-cells) and the excitations (i.e. y_j values, refer eqn. 30) at the *affected taxels* were recorded. However, due to serrated *skin*, R-cells were found to be affected at large. The 'slope' and 'intercept' values of the R-cells were obtained from the corresponding calibration curves. A sample test-data (in mV) is analyzed, which shows *effective excitation* (i.e. x_i values) from six *taxels* (located on three struts, i.e. corresponding to R5, R6 & R9), viz. [(0.256, 0.064), (0.514, 0.128), (0.488, 0.122)]^T, where the data inside each bracket signifies the signals from a single strut. The 'slope' & 'intercept' data for the corresponding struts are [(0.1661, -0.0155), (0.307, -0.0163), (0.3185, -0.0133)]^T (refer eqn. 36). Hence, the computed value of tangential force for each taxel becomes [(1.6152, 0.4038), (1.7168, 0.4292), (1.5648, 0.3912)]^T and the total tangential /*slip force* becomes 6.121 kgf. Considering the coefficient of dynamic friction (µ) between the object and sensor surface to be 0.3, we get the upper limit of the gripping force to be 20.41 kgf., which concludes that the gripper may be loaded with a maximum weight of 12kgf. (approx.).

7.2 Testing with sensor-instrumented jaw gripper

Like earlier case, we consider HEBTEM for checking the condition of presence / absence of object inside the gripper, aided by requisite matrices, viz. 'Y_i' (raw sensor output) and 'N_i' (sensor noise). Each matrix is composed of data, arranged row-wise in increasing order, pertaining to the 18 *active taxels* of the sensory-grid. However, four strain gauge-based force sensor data are not used in the test and data fusion algorithm as well. This has been done deliberately as load cells and strain gauges represent same category of sensor elements; hence those can be treated *homogeneous* from the view-point of data fusion. Hence, in a way

we are only considering 2 *LC-taxels*, 10 *TBS-taxels* and 6 *IR-taxels* in action, as per the layout-schematic given in fig. 20. Although IR-cells are sufficient in their own metric for the purpose of object detection, we adopt the extended sensor model in order to induce redundancy, in case of any malfunction in the IR-cells.

$$u_1 \quad u_2 \quad u_3 \quad u_4 \quad u_5 \quad u_6$$

$$u_7 \quad u_8 \quad u_9 \quad u_{10} \quad u_{11} \quad u_{12}$$

$$u_{13} \quad u_{14} \quad u_{15} \quad u_{16} \quad u_{17} \quad u_{18}$$

Index: {$u_{1,2}$}: LC-taxels; {$u_{3,...,12}$}: TBS-taxels;{$u_{13,...,18}$}: IR-taxels.

Fig. 20. Schematic layout of the taxels in the sensory grid of the gripper

The off-line data for the raw sensory output [Y_i] & system noise [N_i], both expressed in milli-volts are shown below alongwith the computed {u_i} matrix, $\forall$ [$u_i \in (-1,1)$] ,

$$[Y_{ij}] \equiv \begin{bmatrix} 3.93 & 3.89 & 0.0226 & 0.0218 & 0.0245 & 0.0214 \\ 0.0259 & 0.0228 & 0.0234 & 0.0219 & 0.0245 & 0.0227 \\ 429 & 424 & 410 & 407 & 388 & 387 \end{bmatrix} [N_i] \equiv \begin{bmatrix} 0.1 & 0 & 0 & 0.01 & 0 & 0.01 \\ 0.2 & 0 & 0.01 & 0 & 0 & 0.01 \\ 0 & 0.02 & 0.1 & 0 & 0.01 & 0.1 \end{bmatrix} \{u_i\} \equiv \begin{bmatrix} 1 & 1 & 1 & -1 & 1 & -1 \\ 1 & 1 & 1 & -1 & 1 & 1 \\ 1 & 1 & 1 & 1 & -1 & -1 \end{bmatrix}$$

Based on the observation values of the taxels, the computation for the mean global threshold ($\lambda_{Th-mean}$) was done using eqns. 14 & 18 with g(n) = 4(n-1) [i.e. for (p,q) =(1,1)], and finally we got one transcendental equation in 'λ', viz.

$$7.187 x 10^{-5} \lambda^3 - 0.517 \lambda + 12.558 = 0 \tag{37}$$

considering, ξ=0.003; n=18 and α=0.48, in order to solve for '$\lambda_{Th-mean}$'. We need to consider a comparatively larger value of 'α', as the level of uncertainty is more in the preferential selection model, compared to that in additive & multiplicative models. Finally, from eqn. 37, we get the optimized value for '$\lambda_{Th-mean}$' as 27.02 and thenafter, using eqn. 20, the value of the threshold-band becomes 8.16. We observed that in total 13 taxels are giving acceptable signal (i.e. u_i=1) in this testing, barring 5 taxels, vide taxel nos. 4, 6,10,17 & 18. Hence, the computed value of U_G (using eqn. 7) becomes 37, which is more than the mean threshold. Thus, the presence of the object in the gripper-jaw in very well inferred by HEBTEM. Now, based on the 'Y_j' values, pertaining to 18 taxels in order, we can calculate the total tangential force on each jaw (refer eqns. 28 & 29) and finally we can evaluate the final value of the tangential force, averaged over both the jaws. As per fig. 20, the readings {u_3,.., u_6} and {u_7} are mapped to 'F_{t-y}' & 'F_{t-x}' of the left-hand-side jaw respectively and likewise, {u_8,.., u_{11}} and {u_{12}} correspond to 'F_{t-y}' & 'F_{t-x}' of the right-hand-side jaw. Using the data, we get the final average tangential force on the object as η (0.09464) kgf., where 'η' is the calibration coefficient in kgf/mv. Also, {u_1, u_2} is mapped to the grip force on the jaws, which finally amounts to (3.91/M) kgf, where 'M' is the calibration factor, defined in eqn. 27b.

8. Conclusions

A new approach for sensor data fusion of heterogeneous sensor-cells has been described in his article. It proposes a fusion theory wherein the threshold for fusion can be suitably adapted within a finite zone. The threshold estimation for the present work has been based on using *variable threshold*, exploiting the metrics of *Type I* & *Type II* error. The filtered

sensory data is used to estimate the optimal value of the slip force, which is generated in the jaw-object contact zone that ought to be combated for a farm grasp. Nonetheless, HEBTEM also ensures the characteristics of the post-grasp slip, if any.

The proposed schemata provides insight to two aspects, namely evolution of new rule-base towards data fusion and an optimized inference about object's presence or absence based on stochastic hypothesis testing model, using relative dependency of the sensor-cells. HEBTEM has been tested for various objects with different shape, size and contour using the sensor-instrumented gripper and the output is used for processing feedback control signals for its remotized operation, devoid of camera systems.

9. References

Alhakum, S. & Varshney, P.K. (1996). Decentralized Bayesian Detection With Feedback. *IEEE Transactions on Systems, Man & Cybernatics Part A: Systems & Humans*, Vol. SMC-26, No. 4, July 1996, pp 503 – 513, ISSN: 1083-4427.

Chair, Z. & Varshney, P.K. (1986). Optimal Data Fusion in Multiple Sensor Detection Systems. *IEEE Transactions on Aerospace & Electronic Systems*, Vol. AES-22, No. 1, January 1986, pp 98 – 101, ISSN: 0018-9251.

Chen, H.; Kirubarajan, T. & Bar-Shalom, Y. (2003). Performance Limits of Track-to-Track Fusion versus Centralized Estimation: Theory and Application. *IEEE Transactions on Aerospace and Electronic Systems*, Vol. 39, No. 2, April 2003, pp 386 – 400, ISSN: 0018-9251.

Chroust, S.G. & Vincze, M. (2004). Fusion of Vision and Inertial Data for Motion and Structure Estimation. *Journal of Robotic Systems*, Vol. 21, Issue 2, February 2004, pp 73 – 83, ISSN: 0741-2223.

El-Ayadi, M.H. (2002). Nonstochastic Adaptive Decision Fusion in Distributed-Detection Systems. *IEEE Transactions on Aerospace and Electronic Systems*, Vol. 38, No. 4, October 2002, pp 1158 –1171, ISSN: 0018-9251.

Gan, Q. & Harris, C.J. (2001). Comparison of Two Measurement Fusion Methods For Kalman-Filter-Based Multisensor Data Fusion. *IEEE Transactions on Aerospace and Electronic Systems*, Vol. 37, No. 1, January 2001, pp 273 –280, ISSN: 0018-9251.

Gustavo, L.R. & Grajal, J. (2006). Multiple Signal Detection and Estimation using Atomic Decomposition and EM. *IEEE Transactions on Aerospace and Electronic Systems*, Vol. 42, No. 1, January 2006, pp 84 –102, ISSN: 0018-9251.

Hashemi, H.R. & Rhodes, Ian B. (1989). Decentralized Sequential Detection. *IEEE Transactions on Information Theory*, Vol. 35, No. 3, May 1989, pp 509–520. ISSN: 0018-9448.

Jeong, S. & Tugnait, J.K. (2005). Multisensor Tracking of a Maneuvering Target in Clutter Using IMMPDA Filtering with Simultaneous Measurement Update. *IEEE Transactions on Aerospace and Electronic Systems*, Vol. 41, No. 3, July 2005, pp 1122-1131, ISSN: 0018-9251.

Kalandros, M. & Pao, L.Y. (2002). Covariance Control for Multisensor Systems. *IEEE Transactions on Aerospace and Electronic Systems*, Vol. 38, No. 4, October 2002, pp 1138 -1157, ISSN: 0018-9251.

Kalandros, M. & Pao, L.Y. (2005). Multisensor Covariance Control Strategies for Reducing Bias Effects in Interacting Target Scenarios. *IEEE Transactions on Aerospace and Electronic Systems*, Vol. 41, No. 1, January 2005, pp 153 – 173, ISSN: 0018-9251.

Kaplan, L.M. (2006). Local Node Selection for Localization in a Distribued Sensor Network. *IEEE Transactions on Aerospace and Electronic Systems*, Vol. 42, No. 1, January 2006, pp 136 –146, ISSN: 0018-9251.

Karniely, H. & Siegelmann, H.T. (2000). Sensor Registration Using Neural Networks. *IEEE Transactions on Aerospace and Electronic Systems*, Vol. 36, No. 1, January 2000, pp 85 – 101, ISSN: 0018-9251.

Kirubarajan, T.; Wang, H.; Bar-Shalom, Y. & Pattipati, K.R. (2001). Efficient Multisensor Fusion Using Multidimensional Data Association. *IEEE Transactions on Aerospace and Electronic Systems*, Vol. 37, No. 2, April 2001, pp 386 –398, ISSN: 0018-9251.

Lin, X.; Bar-Shalom, Y. & Kirubarajan, T. (2005). Multisensor-Multitarget Bias Estimation for General Asynchronous Sensors. *IEEE Transactions on Aerospace and Electronic Systems*, Vol. 41, No. 3, July 2005, pp 899 – 921, ISSN: 0018-9251.

Moshe Kam; Wei Chang & Qiang Zhu (1991). Hardware Complexity of Binary Distributed Detection Systems With Isolated Local Bayesian Detection. *IEEE Transactions on Systems, Man & Cybernatics*, Vol. SMC-21, No. 3, May-June 1991, pp 565-571, ISSN: 1083-4427.

Moshe Kam; Qiang Zhu & Steven Gray, W. (1992). Optimal Data Fusion of Connected Local Decisions in Multiple Sensor Detection Systems. *IEEE Transactions on Aerospace & Electronic Systems*, Vol. AES-28, No. 3, July 1992, pp 916–920, ISSN: 0018-9251.

Moshe Kam; Chris Rorres; Wei Chang & Xiaoxun Zhu (1999). Performance and Geometric Interpretation For Decision Fusion With Memory. *IEEE Transactions on Systems, Man & Cybernatics, Part A: Systems & Humans*, Vol. 29, No. 1, Jan. 1999, pp 52 – 62, ISSN: 1083-4427.

Murphy, Robin R. (1998). Dempster-Shafer Theory For Sensor Fusion in Autonomous Mobile Robots. *IEEE Transactions on Robotics & Automation*, Vol. 14, No. 2, April 1998, pp 197 – 206, ISSN:1042-296X.

Nabaa, N. & Bishop, R.H (1999). Solution to a Multisensor Tracking Problem with Sensor Registration Errors. *IEEE Transactions on Aerospace and Electronic Systems*, Vol. 35, No. 1, January 1999, pp 354 – 363, ISSN: 0018-9251.

Niu, R.; Varshney, P.K.; Mehrotra, K. & Mohan, C. (2005). Temporally Staggered Sensors in Multi-Sensor Target Tracking Systems. *IEEE Transactions on Aerospace and Electronic Systems*, Vol. 41, No. 3, July 2005, pp 794 – 808, ISSN: 0018-9251.

Okello, N.N. & Challa, S. (2004). Joint Sensor Registration and Track-to-Track Fusion for Distributed Trackers. *IEEE Transactions on Aerospace and Electronic Systems*, Vol. 40, No. 3, July 2004, pp 808 – 823, ISSN: 0018-9251.

Papastavrou, Jason D. & Athans, Michael (1992). Distributed Detection By a Large Team of Sensors in Tandem. *IEEE Transactions on Aerospace & Electronic Systems*, Vol. AES-28, No. 3, July 1992, pp 639 – 652, ISSN: 0018-9251.

Reibman, Amy R. & Nolte, L.W. (1987). Optimal Detection and Performance of Distributed Sensor Systems. *IEEE Transactions on Aerospace & Electronic Systems*, Vol. AES-23, No. 1, Jan. 1987, pp 24 – 30, ISSN: 0018-9251.

Ruan, Y. & Willett, P. (2005). A Quantization Architecture for Track Fusion. *IEEE Transactions on Aerospace and Electronic Systems*, Vol. 41, No. 2, April 2005, pp 671-681, ISSN: 0018-9251.

Sadjadi, Firoz A. (1986). Hypothesis Testing in a Distributed Environment. *IEEE Transactions on Aerospace & Electronic Systems*, Vol. AES-22, No. 2, March 1986, pp 134 – 139, ISSN: 0018-9251.

Srinivasan, R. (1986). Distributed Radar Detection Theory. *IEE Proceedings*, Vol. 133, Part F, No. 1, February 1986, pp 55 – 60, ISSN: 0956-375X.

Swaszek, Peter F. (1993). On the Performance of Serial Networks in Distributed Detections. *IEEE Transactions on Aerospace & Electronic Systems*, Vol. AES-29, No. 1, January 1993, pp 254 – 259, ISSN: 0018-9251.

Tang, Z.B.; Pattipati, K.R. & Kleinman, D.L. (1991). Optimization of Detection Networks: Part I—Tandem Structures. *IEEE Transactions on Systems, Man & Cybernatics*, Vol. SMC-21, No. 5, September / October 1991, pp 1044-1059, ISSN: 1083-4427.

Teneketzis, D. & Varaiya, P. (1984). The Decentralized Quickest Detection Problem. *IEEE Transactions on Automatic Control*, Vol. AC-29, No. 7, July 1984, pp 641-644. ISSN: 0018-9286.

Tenney, Robert R. & Sandell Jr., Nils R. (1981a). Detection With Distributed Sensors. *IEEE Transactions on Aerospace & Electronic Systems*, Vol. AES-17, No. 4, July 1981, pp 501 – 509, ISSN: 0018-9251.

Tenney, Robert R. & Sandell, Nils R. (1981b). Structures For Distributed Decision Making. *IEEE Transactions on Systems, Man & Cybernatics*, Vol. SMC-11, No. 8, August 1981, pp 517 – 527, ISSN: 0018-9251.

Tenney, Robert R. & Sandell, Nils R. (1981c). Strategies For Distributed Decision Making. *IEEE Transactions on Systems, Man & Cybernatics*, Vol. SMC-11, No. 8, August 1981, pp 527 – 538, ISSN: 0018-9251.

Thomopoulos, S.C.A.; Viswanathan, R. & Bougoulias, D.C. (1987). Optimal Decision Fusion in Multiple Sensor Systems. *IEEE Transactions on Aerospace & Electronic Systems*, Vol. AES-23, No. 5, Sept. 1987, pp 644 – 653, ISSN: 0018-9251.

Thomopoulos, S.C.A. (1990). Sensor Integration and Data Fusion. *Journal of Robotic Systems*, Vol. 7, No.3, 1990, pp 337 –372, ISSN: 0741-2223.

Tsitsiklis, John N. & Athans, Michael (1985). On the Complexity of Decentralized Decision Making and Detection Problems. *IEEE Transactions on Automatic Control*, Vol. AC-30, No. 5, May 1985, pp 440 – 446, ISSN: 0018-9286.

Viswanathan, R.; Thomopoulos, S.C.A. & Tumuluri, R.J. (1988). Optimal Serial Distributed Decision Fusion. *IEEE Transactions on Aerospace & Electronic Systems*, Vol. AES-24, No. 4, July 1988, pp 366 – 375, ISSN: 0018-9251.

Wang, X.; Shen, H.C. & Qian, W.H. (1988). A Hypothesis Testing Method For Multi-sensory Data Fusion. *Proceedings of the IEEE International Conference on Robotics & Automation*, pp 3407 – 3412, ISBN: 0-7803-4300-X, Leuven, Belgium, May 1998, IEEE publications, U.S.A., Catalogue No.98CH36146.

Appendix I

Refer to fig. 7. For both multiplicative and additive models, vide eqns. 16 & 17, the required integral is analytically equivalent to the area ABCDE. And, geometrically this area is a *factor* (which is less than 1.0) of the total area, namely ABCD. This rectangular area ABCD is computed from the geometric measure of the sides AB (=CD) and BC (=DA). Using U_G -axis as the common scale for both the plots, we have,

$$\left|\overline{AB}\right| = \left|\overline{CD}\right| = dist\left\{(e^n,0) \quad and \quad (\lambda_{Th.},0)\right\} \equiv (e^{n'} - \lambda_{Th.}) = (e^n - e^{n'}) \text{ [for multiplicative model]}$$

and,

$$\left|\overline{AB}\right| = \left|\overline{CD}\right| = dist\left\{(n,0) \quad and \quad (\lambda_{Th.},0)\right\} = (n - \lambda_{Th.}) \text{ [for additive model]}$$

And, in both the cases using P(H$_1$) axis, we have, $\left|\overline{BC}\right| = \left|\overline{DA}\right| = dist\left\{(0,0) \quad and \quad (1,0)\right\} = 1.0$

Now, for multiplicative model, the required area is '(1-β)' times the area ABCD and for additive model it is '(1-α)' times the area ABCD. Hence we get the deduced expressions on the right-hand-sides of the eqns. 16 & 17.

Sensors: Focus on Tactile Force and Stress Sensors

Edited by Jose Gerardo Rocha and Senentxu Lanceros-Mendez

This book describes some devices that are commonly identified as tactile or force sensors. This is achieved with different degrees of detail, in a unique and actual resource, through the description of different approaches to this type of sensors. Understanding the design and the working principles of the sensors described here requires a multidisciplinary background of electrical engineering, mechanical engineering, physics, biology, etc. An attempt has been made to place side by side the most pertinent information in order to reach a more productive reading not only for professionals dedicated to the design of tactile sensors, but also for all other sensor users, as for example, in the field of robotics. The latest technologies presented in this book are more focused on information readout and processing: as new materials, micro and sub-micro sensors are available, wireless transmission and processing of the sensorial information, as well as some innovative methodologies for obtaining and interpreting tactile information are also strongly evolving.

How to reference

In order to correctly reference this scholarly work, feel free to copy and paste the following:

INTECH
open science | open minds